Theory and Simulation of Jump Dynamics, Diffusion and Phase Equilibrium in Nanopores

Scott M. Auerbach*

Department of Chemistry and Department of Chemical Engineering,
University of Massachusetts, Amherst, MA 01003

Abstract

We review theory and simulation of rare event dynamics, diffusion and phase equilibrium in nanopores, focusing on benzene in Na-X and Na-Y zeolites because of persistent experimental discrepancies. We discuss transition state theory and its application to zeolite–guest systems, suggesting that calculations on flexible lattices and at finite guest loadings are important areas for future research. We consider many-body adsorption and diffusion in zeolites, focusing on the coupling between rare event dynamics and strong guest–guest interactions. We explore the possibility that benzene can undergo phase transitions from low to high sorbate density in Na-X, and find that this type of phase transition might explain intriguing loading dependencies of water and ammonia diffusion in terms of a subcritical droplet picture of adsorption in zeolites. We discuss various formulations of non-equilibrium diffusion through finite lattices, and describe a tracer counter-permeation simulation technique. We find that transport in finite single-file systems is characterized by a diffusivity that decreases monotonically with file length, but that this transport is otherwise completely described by Fick's laws. We conclude by speculating on the prospect for cross-fertilization between zeolite science and other fields.

---

*Email: auerbach@chem.umass.edu

Outline

I. INTRODUCTION

Zeolites are nanoporous crystalline aluminosilicates with a rich variety of interesting properties and industrial applications.[1–3] With over 100 zeolite framework topologies[4,5] synthetically available—each with its own range of compositions—zeolites offer size-, shape- and electrostatically-selective adsorption,[6] diffusion[7,8] and reaction[6] up to remarkably high temperatures. Indeed, the technological importance of zeolites cannot be overstated, considering that the value of zeolite catalysis to petroleum cracking is well in excess of 100 billion dollars.[9] Zeolites are also used as molecular sieves for separating chemical mixtures, as ion exchangers and filters, as environmentally safe detergents, as desiccants for new coolant systems,[10] and as hydrocarbon traps for new cold start catalytic converters.[11] The closely related mesoporous sieves[12] show promise for separating biomolecules, and may be useful for making optical electronic materials with substantial quantum confinement.

As important as zeolites are technologically, the physical chemistry underlying their application is poorly known. The wide-ranging applicability of these materials results from strong zeolite–guest interactions, which can severely retard guest mobility, making theoretical modeling nearly intractable.[13,14] As a result, significant research activity has emerged in the development and application of theoretical methods specialized for rare event dynamics, such as transition state theory and kinetic Monte Carlo, to problems in zeolite science.[15]

In this review, we explore the interplay among rare event dynamics, diffusion and phase equilibrium in nanopores, highlighting our own atomistic simulations and lattice models of molecules in zeolites.[16−35]

Zeolite nomenclature can be confusing despite its attempt at clarity. A given zeolite is typically defined by its three-letter structure type, its silicon to aluminum ratio (Si:Al), and its charge-compensating cations. For example, Na-Y is an "FAU-type" zeolite with a Si:Al > 1.5, and with exchangeable Na cations compensating the negative aluminosilicate framework charge. A different zeolite, Na-X, is also an FAU-type zeolite with Na cations, but with Si:Al < 1.5 and hence containing a higher density of Na cations than that in Na-Y. Other important zeolites include ZSM-5, which is an "MFI-type" zeolite with charge compensated either by Na cations or protons, and silicalite, which is the completely siliceous analog (Si:Al=∞) of ZSM-5. The majority of studies discussed below have been performed on these four zeolites.

We have reported a series of theory and simulation studies modeling rare event dynamics, diffusion and phase equilibrium of benzene in Na-X and Na-Y zeolites,[16−25,27,28,31,33] because of persistent, qualitative discrepancies between different experimental probes of the coverage dependence of self diffusion.[7] We discuss these studies in detail below to provide a common thread for the review. A plethora of other interesting systems exist in zeolite science; our choice of content for the review reflects our own experience in the field, and perhaps our ignorance of other interesting work. We regret that no review can be complete.

We model benzene in Na-X and Na-Y by replacing the zeolite framework with a three dimensional lattice of binding sites. Such a lattice model reproduces behavior accurately when site residence times are much longer than travel times between sites,[36] which is the case for benzene in Na-X and Na-Y because of the strong charge–quadrupole interaction between Na and benzene.[37] The lattice of benzene binding sites in Na-X and Na-Y discussed below contains four tetrahedrally arranged sites inside each cage, as well as four doubly shared, tetrahedrally arranged sites that connect adjacent cages. These intercage sites are typically called "window" sites. Such a hierarchy of intracage and window sites is very common in zeolite science, and is very important for the results described below.

To facilitate visualizing such a complex, three-dimensional lattice, we discuss an analogous two-dimensional lattice shown below. Figure 1 begins with a square lattice of window sites in (a), which are then superimposed on a schematic lattice of zeolite cages in (b), followed by the full lattice including intracage sites in (c). Figure 2 provides a blow-up showing the actual site geometry for benzene in Na-X and Na-Y, including intracage (S_{II}) and window (W) sites. Dynamics and diffusion in this system are strongly influenced by the competition between intracage motion and cage-to-cage migration, which is closely related to the competition between molecular rotation and translation in zeolites. On the other hand, phase transitions in this system are controlled by effective, cage-to-cage attractive interactions that are mediated by the window sites. Below we describe theory and simulation studies on this and related lattice models, with an emphasis on comparison with experiment.

Figure 1. Development of schematic lattice for zeolite–guest systems.

Generic Cage-type Lattice   Benzene in Na-Y

Figure 2. Specific lattice geometry for benzene in Na-Y zeolite.

Lattice models are very convenient for simulating diffusion in zeolites at *low loadings.* However, because the critical temperature of bulk benzene is over 560 K, attractive guest–guest interactions are significant and should not be ignored. Modeling such systems remains challenging because of the coupling between rare event dynamics and strong guest–guest interactions, i.e. the competition between adhesive and cohesive forces. We outline below our recently developed model for determining how guest–guest interactions modify activation energies of site-to-site jumps,[25,31] and speculate on the feasibility of more rigorous dynamical treatments of guest–guest interactions.[38]

In what follows, we review transition state theory and its application to zeolite–guest systems, suggesting that calculations on flexible lattices and at finite guest loadings are important areas for future research. We explore the possibility that benzene can undergo phase

transitions from low to high sorbate density in Na-X, and we discuss various formulations of non-equilibrium diffusion through finite lattices. In general, we find that understanding the thermodynamics of confined fluids can be crucial for elucidating the transport properties of molecules in zeolites, and that explicitly including adsorption and desorption phenomena in open system diffusion models is crucial for drawing qualitatively valid conclusions.

II. TRANSITION STATE DYNAMICS OF SITE-TO-SITE JUMPS IN ZEOLITES

As discussed in the Introduction, the nature of adsorption in nanopores involves some degree of confinement, creating long residence times either in specific sites or more generally in zeolite cages or channels. Atomistic modeling of rare site-to-site or cage-to-cage motions by molecular dynamics (MD) is therefore very challenging. These MD studies have been relegated to relatively weakly binding zeolite–guest systems, and are reviewed in Ref. 14. To model strongly binding zeolite–guest systems, theoretical methods specialized for rare event dynamics, such as transition state theory (TST) and reactive flux correlation theory (RFCT) must be utilized.[39] The challenge in performing these rare event calculations, as with all molecular simulations, is to devise a sufficiently accurate potential energy surface (PES), and to sample statistically relevant regions of the potential.

A. Potentials and Jump Pathways

Most of the molecular simulations performed on zeolite systems to date involve potential functions, i.e. molecular mechanics forcefields. In a small number of studies, the *ab initio* molecular dynamics method of Car and Parrinello[40] has been applied to zeolites;[41–43] because these calculations focus on *very* short time dynamics, we do not discuss them further. The potential functions used in modeling zeolite frameworks generally fall into two categories: ionic models and valence bond models.[44] The ionic models represent the zeolite as a collection of charged species interacting *via* short and long range forces,[45] while the valence bond models represent the zeolite *via* two-body and three-body short range interactions.[14] As with most molecular simulations,[46] short range interactions are only evaluated within a given cut-off distance according to the minimum image convention, while long range forces are evaluated with either the Ewald method[46] or the fast multipole method,[23,47] the choice dictated by the number of atoms allowed to move in the simulation.[23]

Zeolite–guest interactions typically involve Coulombic and Lennard-Jones terms:[16,17,44]

$$V_{\mathrm{ZG}} = \sum_{i=1}^{N_{\mathrm{Z}}} \sum_{j=1}^{N_{\mathrm{G}}} \left\{ \frac{q_i q_j}{r_{ij}} + 4\varepsilon_{ij} \left[\left(\frac{\sigma_{ij}}{r_{ij}} \right)^{12} - \left(\frac{\sigma_{ij}}{r_{ij}} \right)^{6} \right] \right\}, \qquad (2.1)$$

where the charges and Lennard-Jones parameters are fitted to either *ab initio* calculations[48,49] or to crystallographic, adsorption and spectroscopic data. To reduce the complexity of the potential parameter set, further approximations are typically invoked, such as neglecting Lennard-Jones interactions between positively-charged guest atoms and Si/Al frame atoms, because the repulsive electrostatic forces between these atoms supposedly keep them farther

5

apart than the relatively short range of Lennard-Jones interactions. However, recent calculations indicate framework radii of 1.2 Å for Si and 1.0 Å for O,[50] suggesting that Si/Al atoms may protrude into the intracrystalline void space, thereby interacting with guest species at shorter distances than those predicted by conventional wisdom. Further *ab initio* calculations are required to test the severity of neglecting these zeolite–guest Lennard-Jones interactions.

A further approximation that is often invoked involves averaging the properties of Si and Al in the framework, due to the difficulty in quantifying Al distributions in zeolites.[51] This so-called average T-site model, which derives its name from the SiO_4 and AlO_4 tetrahedra in zeolites, may be justified for modeling molecules adsorbed in zeolites when guest atoms remain relatively far from frame atoms, e.g., when guest species interact directly with charge-compensating cations. However, we believe that the average T-site method is unrealistic for modeling cations in zeolites, because of the close proximity between cations and frame atoms. To ameliorate this difficulty, Vitale *et al.* have recently reported a forcefield for Na-X zeolite (Si:Al = 1) using different charges on Si and Al, which accounts for some but not all cation locations in Na-X.[52] Jaramillo and Auerbach have also developed and validated a new forcefield for Na cations in FAU-type zeolites, which explicitly distinguishes Si and Al atoms, as well as different types of oxygens in the framework. This new forcefield gives excellent agreement with experimental data on cation positions, site occupancies and vibrational frequencies for most cations in Na-X and Na-Y.[32]

Despite the complexities of these potentials, they are almost always obtained from *ab initio* or experimental data for species in their stable, equilibrium configurations. However, to use these potentials for modeling rare event dynamics, the potentials must also reproduce energies in the transition state region with equal fidelity. This remains an outstanding problem in Physical Chemistry, which has been addressed for gas phase systems using direct dynamics parameterized by correlated electronic structure methods.[53,54] Along these lines, Truong[55] and Fermann *et al.*[34,35] have performed rate calculations for proton motions in acidic zeolites using various flavors of quantum TST, parameterized directly by correlated electronic structure methods. Unfortunately, such calculations are relegated to *very* small clusters, containing perhaps 3 Si/Al atoms. These small cluster models neglect long range forces,[56] and are likely to overestimate framework rigidity. An important avenue for future research is thus the coupling of direct dynamics methods with periodic electronic structure models of zeolites.[56]

For consistency with the electrostatic treament of zeolite–guest interactions in Eq. (2.1), we prefer in general to use the ionic model with the approximations discussed above, by fitting potential parameters to experimental data. This approach has been used to develop potentials for a wide variety of zeolite–guest systems,[44] including aromatics in FAU-type zeolites such as benzene in Na-Y,[16] Na-X,[17] Ca-X[27] and Si-Y,[57,58] by reproducing sorption sites from crystallography and energies from thermochemistry. Si-Y is the completely siliceous analog of Na-Y, i.e. with no Al and hence no charge-compensating cations, which is synthesized by "Zero Defect De-Alumination" of zeolite Y (ZDDAY).[59] Using these potentials, we have calculated minimum energy paths (MEPs) for site-to-site jumps of benzene in these zeolites, using the constrained optimization technique implemented in our program DIZZY[60] as described in Ref. 16. In addition, other groups have performed MEP calculations for aromatics in FAU-type zeolites.[58,61−63] In general, the agreement between simulation and

experiment is excellent, as discussed below.

To illustrate the results of these MEP calculations, we consider benzene in Na-Y, which has two predominant sites[64] shown schematically in Figs. 2 and 3 In the primary site, denoted as S_{II}, benzene is facially coordinated to a supercage 6-ring, *ca.* 2.7 Å above a Na cation in site II according to crystallographic nomenclature. In the secondary site, denoted as W, benzene lies in the plane of the 12-ring window separating adjacent supercages, *ca.* 5.3 Å from the S_{II} site. Our theory and simulation studies (see Sec. II C) show that the rate determining step for benzene cage-to-cage migration in Na-Y, and hence for intracrystalline diffusion, is the $S_{II} \rightarrow W$ jump, for which the calculated MEP and energies are shown in Fig. 4. The activation energy from these calculations, 41 kJ mol^{-1}, is in excellent agreement with 40±2 kJ mol^{-1}, measured by Isfort *et al.* with two-dimensional exchange NMR.[65] Because this NMR experiment was performed with 5 molecules per Na-Y cage, while our calculation involves 1 molecule per zeolite, it remains unclear whether this favorable comparison is appropriate. Our calculated barrier is also in very good agreement with the unpublished value of 37 kJ mol^{-1}, measured by Jobic using quasi-elastic neutron scattering at low benzene loadings.[66] This computational result provides a picture to go along with these measured activation energies, hence elucidating the process that is actually probed during diffusion measurements.
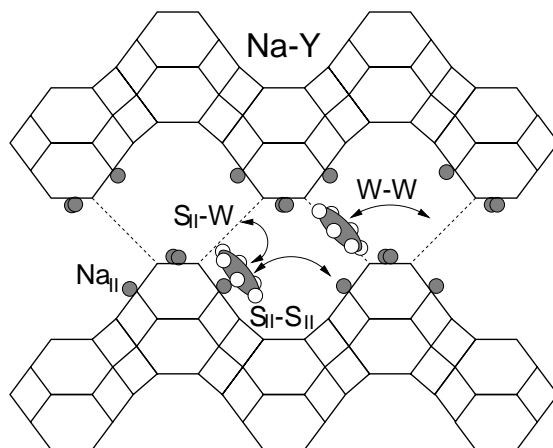

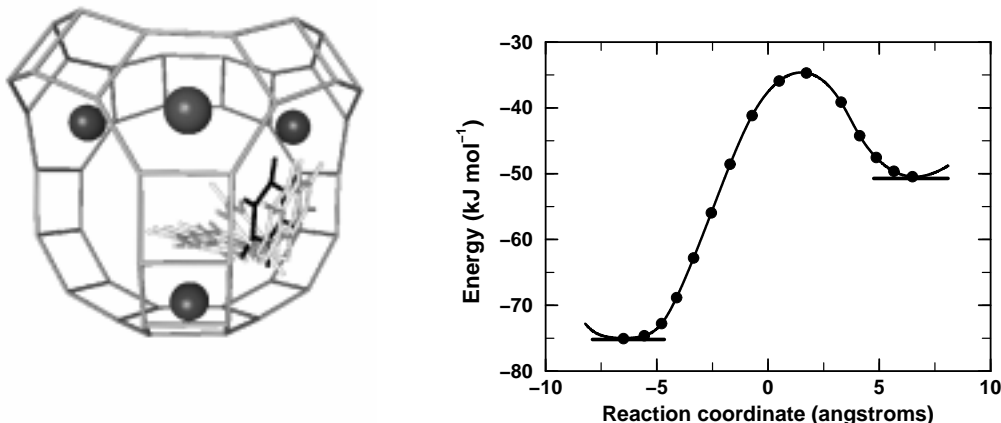Figure 3. Sorption sites and jumps for benzene in Na-Y.

Figure 4. $S_{II} \leftrightarrow W$ MEP for benzene in Na-Y (transition state indicated in bold), with a calculated barrier of 41 kJ mol^{-1}.

In general, we believe this level of accuracy can be obtained for a wide variety of zeolite–guest systems by carefully constructing potentials and searching for transition states. Indeed, Table I shows a comparison between experiment and simulation for benzene in various FAU-type zeolites, where $|\Delta H_{\mathrm{sorb}}|$ is the initial heat of sorption, E_a is the activation energy for intracage motion, and "ref" cites the source of data. The results in Table I show that these potentials are capable of reproducing all the experimental trends in both thermodynamic and kinetic parameters, often with quantitative accuracy.

Zeolite	Exp $|\Delta H_{\mathrm{sorb}}|$	ref	Sim $|\Delta H_{\mathrm{sorb}}|$	ref	Exp E_a	ref	Sim E_a	ref
Ca-X	134	67	119	27	66	68	72	27
Na-X	73	69	70	17	14	17	15	17
Na-Y	79	69	77	16	24	59	35	16
Si-Y	55	58	59	57	10	59	7	57

Table I. Experiment and simulation for benzene energetics (kJ mol^{-1}) in various FAU-type zeolites.

Armed with the success of these potentials, we proceed to calculate pre-exponential factors for rate coefficients describing site-to-site jumps in zeolites. In the next section, we discuss methods for performing transition state theory (TST) and reactive flux correlation theory (RFCT) calculations on molecules in zeolites, illustrating these ideas with results for benzene in Na-Y.

B. Dividing Surface Statistics and Dynamics

The standard *ansatz* in TST is to replace the dynamically converged, net reactive flux from reactants to products with the instantaneous flux through the transition state dividing

surface. TST is inspired by the fact that, although a dynamical rate calculation is rigorously independent of the surface through which fluxes are computed,[70] the duration of dynamics required to converge the net reactive flux is usually shortest when using the transition state dividing surface. The TST approximation can be formulated for gas phase or condensed phase systems,[39,71,72] using classical or quantum mechanics.[73]

The rate coefficient for the jump from site i to site j can be expressed classically as:

$$k_{i \to j}(t) = \frac{1}{\chi_i} \langle \dot{q}(0) \delta_i[\mathbf{r}(0)] \Theta_j[\mathbf{r}(t)] \rangle, \tag{2.2}$$

where χ_i is the equilibrium mole fraction of particles in the state i, q is the particle coordinate perpendicular to the dividing surface bounding state i, $\delta_i[\mathbf{r}]$ denotes the Dirac delta function whose value is 1 if the particle lies on the boundary surface of state i and zero otherwise, and $\Theta_j[\mathbf{r}]$ is the standard step function whose value is 1 if the particle is in state j and zero otherwise. In Eq. (2.2), $\langle \cdots \rangle$ signifies an average in the canonical ensemble.

Equation (2.2) represents the flux of particles flowing through the dividing surface at time 0, weighted by the step function indicating that only those molecules in site j are counted in the average at time t. Although $k_{i \to j}$ depends explicitly on time t in Eq. (2.2), $k_{i \to j}(t)$ will become constant for a finite but reasonably long period of time, provided that site-to-site jumps are truly rare events for the system and temperature of interest. The value of $k_{i \to j}(t)$ in this "plateau regime" is the physically meaningful rate coefficient, which should not depend in principle on the choice of dividing surface. Times in the plateau regime satisfy $\tau_{\mathrm{corr}} < t \ll \tau_{\mathrm{rxn}}$, where τ_{corr} is the typical time of vibrational motion of the particle in its site, and τ_{rxn} is the typical time between two "reactive" events. If the rate coefficient in Eq. (2.2) does not reach a plateau value, but instead decreases linearly with time for a duration long compared with τ_{corr}, then the physically meaningful rate coefficient is obtained by extrapolating this linear descent back to $t = 0$. On the other hand, if neither a plateau regime nor a linear descent can be identified in the time dependence of $k_{i \to j}(t)$, then chemical kinetics is not a useful phenomenology because site-to-site jumps are not rare events. All is not lost, though, because straightforward molecular dynamics can then be used to calculate mobilities.

The standard TST rate coefficient can be written in the same notation:

$$k_{i \to j}^{\mathrm{TST}} = \frac{1}{\chi_i} \langle \dot{q}(0) \delta_i[\mathbf{r}(0)] \Theta_j[\mathbf{r}(\epsilon)] \rangle, \tag{2.3}$$

where ϵ is an infinitesimal time. Unlike Eq. (2.2), here all trajectories that leave site i and enter site j at time 0 are considered reactive; therefore, Eq. (2.3) strongly depends on the exact position of the transition state. The last equation can be rewritten by replacing the projection operator in position with one in velocity, i.e. $\Theta_j[\mathbf{r}(\epsilon)] \to \Theta[\dot{q}(0)]$, yielding the more usual form:

$$k_{i \to j}^{\mathrm{TST}} = \frac{1}{2} \left(\frac{2 k_{\mathrm{B}} T}{\pi m} \right)^{1/2} \frac{Q^{\ddagger}}{Q_i}, \tag{2.4}$$

where k_{B} is Boltzmann's constant, T is temperature, m is the reduced mass associated with the reaction coordinate, $Q^{\ddagger}$ is the configurational partition function on the dividing surface

and Q_i is the configurational partition function in the reactant state i. The last expression can be evaluated without recourse to dynamics, either by Monte Carlo simulation or in the harmonic approximation by normal mode analysis.[74] The exact rate coefficient can then be written as:

$$k_{i \to j} = k_{i \to j}^{\text{TST}} \times f_{ij}(t), \tag{2.5}$$

where the so-called dynamical correction factor is:

$$f_{ij}(t) = \frac{\langle \dot{q}(0)\delta_i[\mathbf{r}(0)]\Theta_j[\mathbf{r}(t)]\rangle}{\langle \dot{q}(0)\delta_i[\mathbf{r}(0)]\Theta_j[\mathbf{r}(\epsilon)]\rangle}. \tag{2.6}$$

The dynamical correction factor is usually evaluated from short molecular dynamics simulations originating on the dividing surface. For classical systems, $f_{ij}(t)$ always takes a value between zero and one, and gives the fraction of initial conditions on the dividing surface that actually lead to reaction at temperature T.

While Eqs. (2.4)–(2.6) are standard expressions of TST and RFCT, the exact way in which they are implemented depends strongly upon the actual system of interest. Indeed, if the transition state dividing surface is precisely known (as for the case of an adatom), Eq. (2.4) then provides a good first approximation to the rate coefficient, and the dynamical correction factor accounts for the possibility that the particle does not thermalize in the state it has first reached, but instead goes on to a different final state. This process is called "dynamical recrossing" if the final state is identical to the original state, and otherwise is called "multisite jumping." The importance of dynamical recrossing or multisite jumping depends on a number of factors, of which the height of the energy barriers and the mechanism of energy dissipation are essential. More important, perhaps, is the fact that the rate coefficient computed *via* Eq. (2.5) does not depend on the exact location of the transition state, as long as the dynamical correction factor $f_{ij}(t)$ can be evaluated with enough accuracy.

In a complex system with many degrees of freedom it might be difficult, or even impossible, to define rigorously the dividing surface between the states. In this case the transition state approximation may fail, requiring the use of Eq. (2.6) or an equivalent expression based on a similar correlation function. Indeed, TST assumes that all trajectories initially crossing the dividing surface in the direction of the product state will eventually relax in this state. This statement will be qualitatively false if the supposed surface does not coincide with the actual dividing surface. In this case, the dynamical correction factor corrects TST for an inaccurately defined dividing surface, even when dynamical recrossings through the actual dividing surface are rare. The problem of locating complex dividing surfaces has recently been addressed using topology,[75] statistics[76] and dynamics.[77,78] These methods share the perspective that complex dividing surfaces can best be understood by considering paths that connect the "reactant" and "product" potential minima.

TST and RFCT have been applied to zeolite–guest systems in a number of interesting studies. These studies were motivated to some extent by the pioneering work of Demontis, Yashonath and Klein,[79] who performed the first molecular dynamics (MD) study on a zeolite–guest system in 1989. In addition to calculating accurate heats of sorption with MD, Demontis *et al.* attempted to use MD to model benzene diffusion in Na-Y at 326 K with a

24 ps long simulation. That the length of their simulation is too short to model diffusion is borne out by their reported diffusion coefficient – 4×10^{-9} m^2 s^{-1} – appropriate for benzene in Si-Y, but 2–3 orders of magnitude too large for benzene in Na-Y.[59]

June, Bell and Theodorou reported the first application of TST dynamically corrected with RFCT for a zeolite–guest system in 1991,[80] modeling the diffusion of Xe and "spherical SF$_6$" in silicalite, the siliceous analog of ZSM-5, an MFI-type zeolite. This system is sufficiently weakly binding that reasonably converged MD simulations could be performed for comparison with the rare event dynamics, showing excellent quantitative agreement in the diffusivities obtained. This study also showed that computers available to academic researchers in the early 1990's can produce a useful overlap between the rare event regime and the molecular dynamics regime. By modeling the motion of spherical guests in silicalite, June *et al.* considerably simplified the task of finding dividing surfaces between sorption sites. The dynamical correction factors obtained by June *et al.* show that recrossings can diminish rate coefficients by as much as a factor of *ca.* 3, and that multisite jumps along straight channels in silicalite[81] contribute to the well known diffusion anisotropy in MFI-type zeolites.[82]

Snurr, Bell and Theodorou then applied harmonic TST to benzene diffusion in silicalite, assuming that benzene and silicalite remain rigid, by using normal mode analysis in generalized coordinates for the 6 remaining benzene degrees of freedom.[83] Their results underestimate experimental diffusivities by one to two orders of magnitude, probably more from assuming a rigid zeolite than from using harmonic TST. Maginn, Bell and Theodorou performed reversible work calculations with a TST flavor on long chain alkanes in silicalite,[84] finding that diffusivities monotonically decrease with chain length until about n-C$_8$, after which diffusivities plateau and become nearly constant with chain length. Greenfield and Theodorou even dared to apply TST to model molecular penetration through glassy polymers, by computing configurational averages involving *ca.* 350 degrees of freedom.[85] They found an extremely broad distribution of rate coefficients for methane jumps in atactic polypropylene at 233 K.

Jousse and co-workers reported a series of MD studies on butene isomers in channel zeolite-types MEL and TON.[26,86] Because the site-to-site energy barriers in these systems are comparable to the thermal energies studied in the MD simulations, rare event dynamics need not apply. Nonetheless, Jousse and co-workers showed that even for these relatively low-barrier systems, the magnitudes and loading dependencies of the MD diffusivities could be well explained within a jump diffusion model, with residence times extracted from the MD simulations. These studies show once again that with modern computers, the MD regime and rare event regime can have significant overlap.

Mosell, Schrimpf and Brickmann reported a series of TST and RFCT calculations on Xe in Na-Y[87,88] in 1996, and benzene and p-xylene in Na-Y[63,89] in 1997. They calculated the reversible work of dragging a guest specie along the cage-to-cage [111] axis of Na-Y, and augmented this version of TST with dynamical corrections. In addition to computing the rate coefficient for cage-to-cage motion through Na-Y, Mosell *et al.* confirmed that benzene W sites are free energy local minima, while p-xylene W sites are free energy maxima, i.e. cage-to-cage transition states.[63,89] Mosell *et al.* also found relatively small dynamical correction factors, ranging from 0.08–0.39 for benzene and 0.24–0.47 for p-xylene. At about the same time in 1997, Jousse and Auerbach reported TST and RFCT calculations of specific site-to-

site rate coefficients for benzene in Na-Y,[23] using Eq. (2.2) with jump-dependent dividing surfaces (see Fig. 5 below). As with Mosell *et al.*, we found that benzene jumps to W sites could be defined for all temperatures studied. We found dynamical correction factors mostly above 0.5, suggesting that our jump-dependent dividing surfaces coincide more closely with the actual ones. Although the flavors of the two approaches for modeling benzene in Na-Y differed, the final results were remarkably similar considering that different forcefields were used. In particular, Mosell *et al.* used MD to sample dividing surface configurations, while we applied the Voter displacement-vector Monte Carlo method[90] for sampling dividing surfaces. The apparent activation energy for cage-to-cage motion in our study is 44 kJ mol^{-1}, in very reasonable agreement with 49 kJ mol^{-1} obtained by Mosell *et al.* Below we discuss further the results in Ref. 23, to illustrate these TST and RFCT calculations.

As a prelude to our discussion of many-body diffusion in Sec. III, we note that Tunca and Ford have reported TST rate coefficients for Xe cage-to-cage jumps at high loadings in ZK-4 zeolite, the siliceous analog of Na-A, an "LTA-type" zeolite.[38] These calculations deserve several remarks. First, because this study treats multiple Xe atoms simultaneously, defining the reaction coordinate and dividing surface can become quite complex. Tunca and Ford addressed this problem by considering averaged cage sites, instead of specific intracage sorption sites, which is valid because their system involves relatively weak zeolite–guest interactions. They further assume a one-body reaction coordinate and dividing surface regardless of loading, which is tantamount to assuming that the window separating adjacent α-cages in ZK-4 can only hold one Xe at a time, and that cooperative many-Xe cage-to-cage motions are unlikely. Second, Tunca and Ford advocate separate calculations of $Q^{\ddagger}$ and Q_i for use in Eq. (2.4), as opposed to the conventional approach of calculating ratios of partition functions *viz.* free energies.[90] It is not yet obvious to the author whether separating these calculations is worth the effort. Third, Tunca and Ford have developed a recursive algorithm for building up $(N + 1)$-body partition functions from N-body partition functions, using a "test particle" method developed for modeling the thermodynamics of liquids. Although the approach of Tunca and Ford has a restricted regime of applicability, and is not yet able to compare with experiment, it nonetheless seems promising in its direct treatment of many-body diffusion effects.

To illustrate the mechanics of TST and RFCT calculations, we discuss our results for benzene in Na-Y.[23] We calculated rate coefficients for the following jumps: $S_{II}\rightarrow S_{II}$, $S_{II}\rightarrow W$, $W\rightarrow S_{II}$ and $W\rightarrow W$ (see Figs. 3 and 4). The dividing surfaces used for these jumps are shown schematically in Fig. 5. These surfaces are justified by a number of features of the actual sites: (*i*) the symmetry of the $S_{II}\rightarrow S_{II}$ and $W\rightarrow W$ paths requires the corresponding dividing surface to be on the symmetry plane; (*ii*) the transition state for the $S_{II}\rightarrow W$ jump happens to lie near the line joining the S_{II} and W sites. Figure 5 shows that a problem appears for the $W\rightarrow W$ jump: the dividing surface is indeed reduced to naught by the $W\rightarrow S_{II}$ dividing planes. This does not mean that there is actually no dividing surface, but only that it cannot be defined in as simple and logical a way as for the $S_{II}\rightarrow S_{II}$ and $S_{II}\rightarrow W$ processes. Boundaries were placed on the W-W symmetric plane on each side in the middle 4-ring, so that its total extent amounts to 2.4 Å. To extend the boundary surface farther would cause it to approach the S_{II} site, which is not a possible transition state for the $W\rightarrow W$ jump.
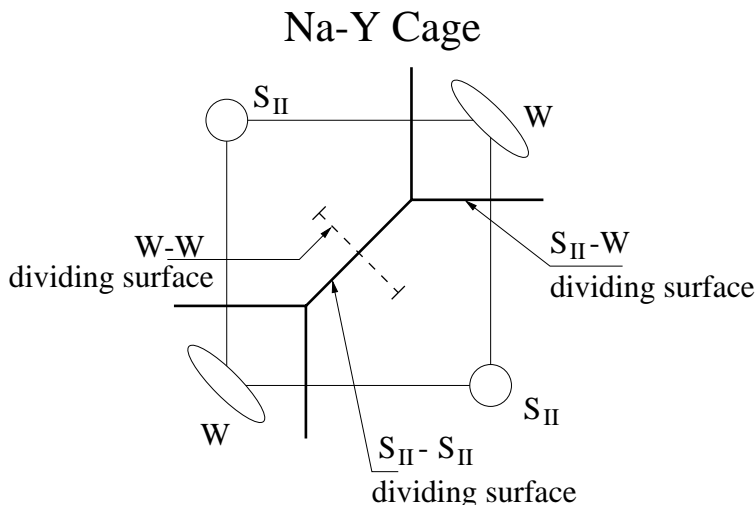
Figure 5. Schematic of dividing surfaces for benzene jumps in Na-Y.

In general, dividing surfaces for benzene jumps should involve no fewer than 5 degrees of freedom, to account for benzene's orientational anisotropy. Our dividing surfaces clearly ignore this anisotropy, which could lead to sizable error in the TST rate coefficients. To test this, we calculated TST rates by averaging over 200,000 Monte Carlo steps in both the reactant and transition state. The corresponding dynamical correction factors were calculated by averaging over 2,000 MD trajectories initialized on the dividing surface, and propagated for *ca.* 10 ps or until final thermalization was confirmed. A typical TST calculation for this system required 10 CPU hours on an IBM RS/6000 PowerPC 604e 200MHz processor, while the corresponding dynamical correction required *ca.* 48 additional CPU hours. Figure 6 shows the time dependence of the dynamical correction factor for the $S_{II} \rightarrow S_{II}$ jump at 298 K. In general, $f_{ij}(t)$ should start at 1 and decrease non-monotonically to the plateau value. In Fig. 6, the initial rise of $f_{ij}(t)$ is an artifact of the calculation, due to the fact that our dividing surface has a width,[90] set in this calculation to 0.2 Å. The behavior of $f_{ij}(t)$ agrees well with what has been described in the literature: after an initial rapid decay, $f_{ij}(t)$ decays very slowly to its plateau value, in this case 0.687. We have also confirmed that the RFCT results are independent of dividing surface, while the TST rates depend strongly on dividing surface location, by redoing the calculations using a slightly different transition state.
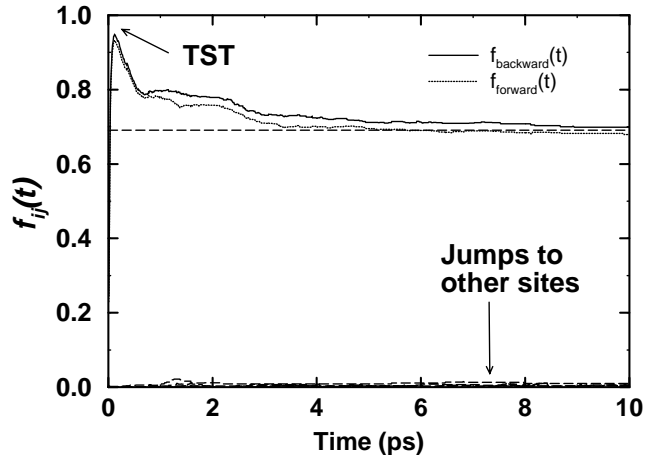
Figure 6. Time dependence of the dynamical correction factor for the $S_{II} \rightarrow S_{II}$ benzene jump in Na-Y at 298 K.

The fact that the dynamical correction factor for the $S_{II} \rightarrow S_{II}$ rate coefficient plateaus near 0.7 suggests that neglecting benzene's anisotropy in defining the $S_{II} \rightarrow S_{II}$ dividing surface is reasonable. To determine if the other dividing surfaces for benzene in Na-Y work as well, we calculated TST and RFCT rates for all 4 jumps over the temperature range 150–500 K. The resulting apparent activation energies and pre-exponential factors are shown in Table II, along with the apparent Arrhenius parameters for the $S_{II} \rightarrow W$ equilibrium coefficient.

| | Activation Energy (kJ mol^{-1}) | | | Arrhenius Prefactors | |
Jump Process	MEP	TST	RFCT	TST	RFCT
$W \rightarrow S_{II}$	16	17.0 ± 0.1	16.4 ± 0.3	$2.7 \ 10^{12} \ s^{-1}$	$1.1 \ 10^{12} \ s^{-1}$
$W \rightarrow W$	18	$\rightarrow 1.1 \pm 0.5 \leftarrow$	15.1 ± 4.0	$6.0 \ 10^{11} \ s^{-1}$	$2.4 \ 10^{11} \ s^{-1}$
$S_{II} \rightarrow W$	41	44.8 ± 0.1	44.4 ± 0.1	$1.6 \ 10^{13} \ s^{-1}$	$0.8 \ 10^{13} \ s^{-1}$
$S_{II} \rightarrow S_{II}$	35	37.4 ± 0.1	36.8 ± 0.3	$1.6 \ 10^{13} \ s^{-1}$	$0.8 \ 10^{13} \ s^{-1}$
$K_{eq}(S_{II} \rightarrow W)$	25	28.0 ± 0.2		7.1	

Table II. Apparent Arrhenius parameters from rate coefficients for benzene jumps among S_{II} and W sites in Na-Y, using TST and RFCT methods. Note the failure of TST for the $W \rightarrow W$ jump.

Several remarks can be made about the data in Table II. First, the equilibrium coefficient energetically favors the S_{II} site for its strong $\pi-$cation interaction, but entropically favors the W site for its greater flexibility; a trend that is mirrored by the rate coefficients. This entropic predisposition for the W site is important for benzene phase transitions in Na-X,[28] discussed in Sec. III B. Second, we clearly see the failure of TST for modeling the $W \rightarrow W$ process, not because TST is inaccurate, but rather because our implementation of TST does not account for the anisotropy of the actual $W \rightarrow W$ dividing surface. Third, because the $W \rightarrow W$ prefactor is nearly an order of magnitude smaller than that for the $W \rightarrow S_{II}$ jump, there is likely to be a strong entropic bottleneck in the $W \rightarrow W$ jump. This can arise from either a tight transition state, which TST should be able to handle, or from other final states

14

that lie close to the W→W dividing surface, which TST *cannot* treat accurately because of its blindness to the eventual fate of dividing surface flux. Figure 5 shows that the W→W path crosses right through the S_{II}→S_{II} path, suggesting that most of the flux through the W→W dividing surface relaxes to an S_{II} site. Thus, most of these W→W dividing surface configurations have nothing to do with actual W→W jumps, but do have energies slightly higher than the W site energy, explaining the very small TST activation energy for this jump.

Before leaving this section, we address a question that is raised at every meeting on zeolite science: What effect do lattice vibrations play in molecular jump dynamics? While we cannot provide a comprehensive answer, we can suggest some guidelines.[14,91] For guest molecules that fit tightly into zeolite pores, molecular simulations that neglect lattice vibrations will almost surely overestimate cage-to-cage jump activation energies, because rigid-lattice simulations ignore the cooperative effect of ring breathing with molecular motion. Such an error in the activation energy will produce rate coefficients that can be several orders of magnitude too small, as Snurr *et al.* found for benzene in silicalite.[83] For guest molecules that fit loosely into zeolite pores, rigid-framework MD or TST simulations are likely to overestimate the external vibrational frequencies of guests during site-to-site jump attempts, because keeping the framework rigid hardens the vibrational environment of an adsorption site. Such an error in attempt frequencies is not likely to produce order-of-magnitude errors in rate coefficients or diffusion coefficients, because rates and diffusivities are only linearly proportional to attempt frequencies.[80] To examine these effects, we performed several TST calculations allowing for benzene internal flexibility and/or Na vibration in Na-Y zeolite.[91] A typical TST calculation with flexible benzene and movable Na cations required 35 CPU hours on an IBM PowerPC. These TST calculations show only 1 kJ mol^{-1} decreases in activation energies, and very modest changes in pre-exponential factors.

We thus find that site-to-site jump dynamics in zeolites are well described by TST when the initial or final sites involve relatively deep potential mimina, and that molecular jump dynamics in a large pore zeolite is well described by including only a small number of degrees of freedom. We now turn our attention to calculating observable mobilities arising from molecular translation and rotation.

C. Diffusion and Orientational Randomization at Infinite Dilution

In order to make contact with measurements of transport through zeolites,[7,8] we must relate our site-to-site rate coefficients with quantities such as the self diffusivity and transport diffusivity, which arise from molecular translation; or we can model NMR correlation times, which are controlled by molecular rotation. At infinite dilution on an M-dimensional hypercubic lattice, i.e. 1-d, 2-d square, 3-d cubic, etc., both the self and transport diffusivity are given by $D_0 = k_{\text{hop}} a^2 = \frac{1}{2M} k a^2$, where k_{hop} is the rate coefficient for jumps between nearest neighbor sites, a is the distance between such sites, and $1/k$ is the mean site residence time.[36] This result neglects multisite hops, which have jump distances greater than a. Unfortunately, site lattices in zeolites are much more complicated than hypercubic, apparently defying such simple analytical formulas. To address this complexity, many researchers have applied kinetic Monte Carlo (KMC) to modeling diffusion in zeolites, parameterized either

by *ad hoc* jump frequencies or by atomistically calculated jump rate coefficients.

KMC models diffusion on a lattice as a random walk composed of uncorrelated, single molecule jumps. KMC is isomorphic to the more conventional Monte Carlo algorithms,[46] except that in a KMC simulation random numbers are compared to ratios of rate coefficients, instead of ratios of Boltzmann factors. However, if the pre-exponential factors cancel in a ratio of rate coefficients, then a ratio of Boltzmann factors does arise, where the relevant energies are *activation energies.* In addition to modeling transport in zeolites, KMC has been used to model adsorption kinetics on surfaces,[92] and even surface growth itself.[93] The fundamental assumption in KMC is that successive jumps are uncorrelated, leading to a Poisson distribution of jump times controlled by the pre-calculated rate coefficients. This assumption can break down when many-body motions become correlated, as can happen with polymer dynamics or surface reconstructions.[77] Despite these concerns, KMC remains a powerful technique for modeling jumps of neutral molecules in zeolites.

KMC can be implemented with constant time-step algorithms where jumps are accepted or rejected based on the kinetic Metropolis prescription, in which a ratio of rate coefficients, $k_{\text{hop}}/k_{\text{ref}}$, is compared to a random number.[19,94] Here k_{ref} is a reference rate that controls the temporal resolution of the calculation. KMC can also be implemented with variable time-step algorithms, in which a hop is made every KMC step and the system clock is updated accordingly.[95,96] The mean time elapsed before each hop is the inverse of the *total* rate coefficient to leave the originating site. In all cases, the probability of a particular jump is proportional to the associated rate coefficient. We find that constant time-step KMC is more convenient for calculating correlation functions, while variable time-step KMC is more efficient for calculating mean square displacements.[19]

Most KMC simulations of diffusion in zeolites are performed at high guest loadings, to explore the effects on transport of guest–guest interactions. We review these studies below in Sec. III. A handful of studies have been reported modeling diffusion in zeolites at infinite dilution with KMC, to relate fundamental rate coefficients with observable self diffusivities for particular lattice topologies. June *et al.* augmented their TST and RFCT study with KMC calculations of Xe and SF_6 self diffusivities in silicalite.[80] They obtained excellent agreement among apparent activation energies for Xe diffusion calculated using MD, KMC with TST jump rates, and KMC with RFCT jump rates. The resulting activation energies fall in the range 5–6 kJ mol^{-1}, which unfortunately is much lower than the experimentally determined values of 15 and 26 kJ mol^{-1}.[97,98] van Tassel *et al.* reported a similar study in 1994 on methane diffusion in zeolite A, finding excellent agreement between self diffusivities calculated with KMC and MD.[99] Auerbach *et al.* reported KMC simulations of benzene diffusion in Na-Y, showing that the $S_{\text{II}} \rightarrow W$ jump controls the temperature dependence of diffusion,[16] as discussed further below. Because benzene residence times at S_{II} sites are so long, these KMC studies could not be compared directly with MD, but nonetheless yield very good agreement when compared with experiment (see Sec. II A).

KMC simulations of diffusion in zeolites at infinite dilution usually involve a relatively small configuration space, and a modest number of input parameters. The results of KMC for sufficiently simple systems can often be anticipated, e.g. the apparent activation energy for self diffusion in zeolites is usually controlled by jumping through a zeolite window. Indeed, consider the case of benzene in Na-Y. Because the lattice of supercages is a diamond lattice, as shown in Fig. 2, we can simplify the motion of benzene in Na-Y by imagining that—

although hops really take place among S_{II} and W sites—long range motion involves jumps from one "cage site" to an adjacent "cage site."[18,20,100−102] As such, all the S_{II} and W site structure within a cage becomes the internal structure of the cage site. A random walk through Na-Y reduces to hopping on the tetrahedral lattice of supercages, for which the mean square displacement after N cage-to-cage jumps is given by:

$$\left\langle R^2(N) \right\rangle = \left\langle \left| \sum_{i=1}^{N} \vec{l}_i \right|^2 \right\rangle = \left\langle \sum_{i=1}^{N} \left| \vec{l}_i \right|^2 \right\rangle + \left\langle \sum_{i \neq j} \vec{l}_i \cdot \vec{l}_j \right\rangle \tag{2.7}$$

$$= \left\langle \sum_{i=1}^{N} a^2 \right\rangle = Na^2 = kta^2 = 6D_s t,$$

where a is the kinetically averaged cage-to-cage distance, and $1/k \equiv \langle \tau_c \rangle$ is the kinetically averaged supercage residence time.[18] The third equality results because jumps are uncorrelated, and the final equality establishes that $D_s = \frac{1}{6} k a^2$, identical to the expression for a simple-cubic lattice. The same result is obtained from a rigorous analysis of the random walk average using Bernoulli statistics,[18] which explicitly samples the eight possible random jump vectors $\{\vec{l}_i\}$ for a tetrahedral lattice. In fact, the same result is obtained for any regular lattice in three dimensions consisting of only one site type and one jump length scale, *viz.* the tetrahedral lattice.

Now we seek analytical formulas for k and a in terms of fundamental rate coefficients and jump lengths for the lattice model of benzene in Na-Y. The mean cage-to-cage jump distance does have a weak temperature dependence,[18] but nonetheless remains close to the cage-center to cage-center distance, *ca.* 10.8 Å.[64] The supercage residence time is more interesting, however. In what follows the W and S_{II} sites are denoted sites 1 and 2, respectively.

We imagine a trajectory executed by a single benzene molecule through Na-Y, hopping among S_{II} and W sites. In the limit of a *very* long trajectory, mean residence times at S_{II} and W sites can be used to calculate hopping rate coefficients and equilibrium coefficients in accord with the ergodic hypothesis.[103] The mean supercage residence time is then given by:

$$\langle \tau_c \rangle = \frac{T}{N_{cc}} = \frac{1}{N_{cc}} (T_1 + T_2) = \frac{T_1}{N_{cc}} \left(\frac{T_1 + T_2}{T_1} \right)$$

$$\xrightarrow{T \to \infty} \frac{T_1}{N_{cc}} \left[1 + K_{eq}(1 \to 2) \right], \tag{2.8}$$

where $T = T_1 + T_2$ is the total time of the trajectory, T_1 and T_2 are the total residence times at W and S_{II} sites, respectively, and N_{cc} is the number of cage-to-cage jumps during the trajectory. The long time limit in Eq. (2.8) ensures convergence of T_2/T_1 to the equilibrium coefficient $K_{eq}(1 \to 2) = 2k_{1 \to 2}/k_{2 \to 1}$, where $k_{i \to j}$ are fundamental rate coefficients (*cf.* Table II), and the factor of two arises because each W site is shared between two adjacent supercages. The long time limit allows T_1 to be expressed as:

$$T_1 = N^\ddagger \cdot \frac{T_1}{N^\ddagger} = N^\ddagger \cdot \langle \tau_1 \rangle$$

$$\xrightarrow{T \to \infty} \frac{N^\ddagger}{k_1} = \frac{N^\ddagger}{6 \left(k_{1 \to 1} + k_{1 \to 2} \right)}, \tag{2.9}$$

17

where $N^{\ddagger}$ is the number of visits to W sites, $\langle\tau_1\rangle$ is the mean W site residence time, $k_1 = 1/\langle\tau_1\rangle$ is the total rate of leaving the W site, and the factor of six counts available target sites in the Na-Y supercage structure. The long trajectory limit allows one further simplification, namely that $N_{cc} = N^{\ddagger}/2$. The factor of one half accounts for randomizing in the W site which halves the probability to leave the cage, an assumption which is valid for benzene but not p-xylene in Na-Y.[63]

Putting these results together, we have:

$$\langle\tau_c\rangle = 2 \cdot \langle\tau_1\rangle \cdot [1 + K_{eq}(1 \rightarrow 2)] = \frac{1 + 2k_{1\rightarrow2}/k_{2\rightarrow1}}{3\,(k_{1\rightarrow1} + k_{1\rightarrow2})}, \qquad (2.10)$$

which represents an exact formula determining cage-to-cage motion in terms of fundamental hopping rate coefficients. The formula in Eq. (2.10) agrees quantitatively with results from KMC simulations for all temperatures and fundamental rate coefficients studied.[18,20] If we assume that $K_{eq}(1 \rightarrow 2) \gg 1$ because of the energetic stability of the S_{II} site, the cage-to-cage rate coefficient reduces to:

$$k \cong \frac{3}{2} \cdot k_{2\rightarrow1}\left(1 + \frac{k_{1\rightarrow1}}{k_{1\rightarrow2}}\right) \cong \frac{3}{2}k_{2\rightarrow1}, \qquad (2.11)$$

where the last approximation arises from the entropically diminished pre-exponential for the W→W jump. Thus, we have found that the rate-determining step for cage-to-cage migration, and hence intracrystalline self diffusion for benzene in Na-Y is the S_{II}→W jump. Qualitatively similar conclusions can be expected for many other zeolite–guest systems, but not for long chain alkanes ($> C_8$) in FAU-type zeolites, which are dominated by W→W jumps.[104]

The diffusion theory outlined above in Eqs. (2.7)–(2.11) relies on the tetrahedral topology of Na-Y in particular, and FAU-type zeolites in general. Developing such a theory for general frameworks remains challenging. Braun and Sholl have recently developed a Laplace-Fourier transformation method for calculating exact self-diffusion tensors in generalized lattice gas models.[105] These methods in general involve quite heavy matrix algebra, which can sometimes hide the underlying physical meaning of the parameters. Jousse, Auerbach and Vercauteren have developed an alternative method for deriving analytical self-diffusion coefficients at infinite dilution for general lattices, by partitioning the correlated displacement of a tracer into uncorrelated sequences of jumps.[33] This approach can be used to analyze both geometric correlations due to the non-symmetric nature of adsorption sites in zeolite pores, and kinetic correlations arising from insufficient thermalization of a molecule in its final site.

It is interesting to note that the formulas controlling cage-to-cage motion are rigorously independent of $k_{2\rightarrow2}$, the S_{II}→S_{II} rate coefficient. As such, a measurement of benzene diffusion through Na-Y is totally insensitive to this fundamental rate parameter, raising the question: What physical situation would be controlled by the intracage, S_{II}→S_{II} hopping process? We have addressed this issue by performing KMC simulations of the orientational correlation function (OCF) that is probed by NMR relaxation and multidimensional exchange experiments,[106] namely $C(t) = \langle P_2(\cos\beta_t)\rangle$, where $P_2(x) = \frac{1}{2}(3x^2 - 1)$ is the second-degree Legendre polynomial, and β_t is the angle between benzene's six-fold axis at time 0

and t. We note that Klein *et al.* studied this OCF and others in their molecular dynamics simulations of benzene, xylenes and nitroaniline in Na-Y.[107] We have found that benzene orientational randomization in Na-Y is controlled exclusively by $k_{2\rightarrow2}$ when the Si:Al ratio of the zeolite provides full occupancy of Na(II) cations.[19] Because these Na(II) cations are arranged tetrahedrally in the supercage, as shown in Fig. 2, benzene can undergo complete orientational randomization by making only $S_{II}\rightarrow S_{II}$ jumps, and by avoiding the more energetically costly $S_{II}\rightarrow W$ jump. Thus, we predict that the NMR spin-lattice relaxation experiments of Bull *et al.*[59] on benzene in Na-Y (Si:Al=1.7) observe intracage hopping processes, their data providing a direct probe of the $S_{II}\rightarrow S_{II}$ hopping rate coefficient. This suggests the comparison of their 24 kJ mol^{-1} apparent activation energy to our $E_a(S_{II}\rightarrow S_{II})$ = 35 kJ mol^{-1}, as shown in Table I.

In several instances self diffusion coefficients for adsorbed benzene are estimated from relaxation data[59,108–110] according to $D_s \sim \frac{1}{6}k_{BOR}a^2$, where a is a likely jump length chosen from structural data, and $1/k_{BOR}$ is the measured correlation time for benzene orientational randomization (BOR). Our present results suggest that using NMR relaxation data to estimate diffusivities may be incorrect for many systems. Therefore, reporting NMR correlation times in terms of diffusion coefficients may lead to inappropriate comparisons with data from, e.g., pulsed field gradient (PFG) NMR which directly measures mean square displacements.[7,111]

These results indicate that benzene intracage dynamics in Na-Y can be probed by measuring molecular rotation with NMR relaxation; while intercage dynamics requires a probe of molecular translation, which can be achieved with PFG NMR. One wonders whether a single experiment can measure both intracage and intercage dynamics. We have addressed this question by modeling BOR in Na-Y with only 2 Na(II) cations per supercage, thereby breaking the tetrahedral symmetry that was present with 4 Na(II) cations per cage.[19] Our KMC calculated OCF exhibits biexponential decay as shown in Fig. 7, revealing rapid intracage motion ($S_{II}\rightarrow S_{II}$) at short times and more sluggish cage-to-cage migration ($S_{II}\rightarrow W$) at longer times. This prediction has been verified experimentally for benzene in Ca-Y (Si:Al=2.0) by the exchange-induced sidebands NMR method,[27] hence providing a single experiment that can probe simultaneously intracage and intercage motions in zeolites.
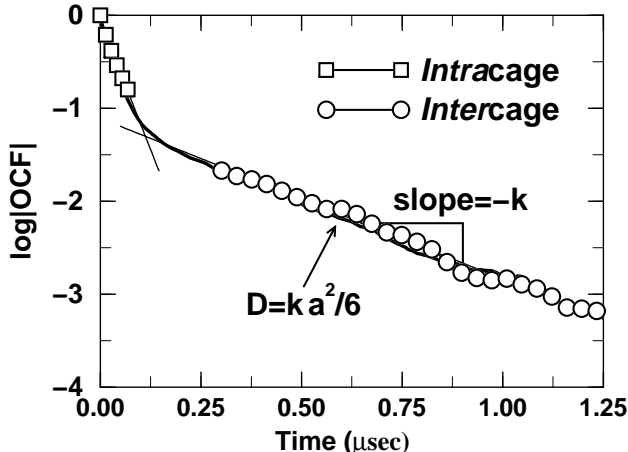
Figure 7. Ln|OCF| for benzene in Na-Y (Si:Al=3.0) at $T = 300$ K by KMC. Intracage motion gives rapid, incomplete decay while cage-to-cage migration gives slower, long time decay.

By modeling BOR in Na-Y with only 1 Na(II) cation per supercage, we have found that the resulting OCF is sensitive to the precise distribution of Na(II) cations.[19] In particular, single exponential decay of the OCF is predicted when each cage contains exactly 1 Na(II) cation, while biexponential decay arises when the distribution of Na(II) cations among supercages is not as regular. This is important because measuring the distribution of Na(II) cations is closely related to measuring Al distributions in disordered zeolites, which remains challenging to modern characterization methods.[51,112] The striking conclusion drawn from these calculations is that studying BOR in Na-Y with one quarter Na(II) occupancy can clearly distinguish between qualitatively different Al distributions. We therefore suggest that guest mobility can be used to probe structural aspects of disordered zeolites; this prediction awaits experimental verification.

Thus far our discussion of dynamics in zeolite has focused (almost[38]) exclusively in the low loading regime, wherein the transport of isolated guest molecules can be considered. This is the least interesting situation to those who utilize zeolites in chemical applications, because infinite dilution means slowly accumulating profits. In Sec. III, we turn our attention to the statistical mechanical problem of many-body diffusion in zeolites.

III. STATISTICAL MECHANICS OF MANY-BODY DIFFUSION IN ZEOLITES

Significant effort has been devoted to understanding the loading dependence of diffusion in zeolites, revealing fascinating physical effects such as anomalous diffusion,[113,114] correlated cluster dynamics,[115] soft core interactions,[21,25] broken symmetry[27] and percolation.[116] Most if not all models of the loading dependence of jump diffusion in zeolites have been carried out with KMC. Variable time-step KMC simulations are usually carried out as follows: for a given configuration, $\vec{n}$, of random walkers, a process list of possible hops from occupied to empty sites is compiled for all molecules. A particular jump from site i to j is chosen from this list with a probability of $k_{i \rightarrow j}/k_{\text{tot}}(\vec{n})$, where $k_{i \rightarrow j}$ is the i to j rate coefficient and $k_{\text{tot}}(\vec{n})$ is the sum of all rate coefficients in the process list. A hop is made every KMC step and the system clock is updated with variable time-steps.[95,96] The actual KMC time-step is obtained from: $\Delta t(\vec{n}) = -\ln(1-x_1)/k_{\text{tot}}(\vec{n})$, where $x_1 \in [0,1)$ is a uniform random number.

The great challenge in implementing this scheme is that the rate coefficients $\{k_{i \rightarrow j}\}$ should depend upon the local configuration of molecules because of guest–guest interactions. That is, in compiling the process list of allowed jumps and associated rate constants on the fly of a KMC simulation, TST or RFCT calculations should be performed to account for the effect of specific guest configurations on the jump rate coefficients. This scheme could become feasible if rate coefficients for jumps within recurring configurations are stored and efficiently accessed for subsequent KMC steps. To date, this "*ab initio* many-body KMC" approach has not been employed because of its daunting computational expense. Instead, researchers either ignore how guest–guest interactions modify rate coefficients for site-to-site jumps; or they use many-body MD at elevated temperatures when guest–guest interactions cannot be ignored.[77,78]

A popular approach for modeling many-body diffusion in zeolites with KMC is thus the "site blocking model," where guest–guest interactions are ignored, except for exclusion of multiple site occupancy. This model accounts for entropic effects of finite loadings, but not energetic effects. Calculating the process list and available rate coefficients becomes particularly simple; one simply sums the available processes using rates calculated at infinite dilution.[22] This model is attractive to researchers in zeolite science,[117] because blocking of cage windows and channels by large, aromatic molecules that form in zeolites, i.e. "coking," is a problem that zeolite scientists need to understand and eventually eliminate.

Theodorou and Wei used KMC to explore a site blocking model of reaction and diffusion with various amounts of coking.[118] Nelson and co-workers developed similar models, to explore the relationship between the catalytic activity of the zeolite and its lattice percolation threshold.[119,120] In a related study, Keffer, McCormick and Davis modeled binary mixture transport in zeolites, where one component diffuses rapidly while the other component is trapped at sites, e.g. methane and benzene in Na-Y.[116] They used KMC to calculate percolation thresholds of the rapid penetrant as a function of blocker loading, and found that these thresholds agree well with predictions from simpler percolation theories.[121] Coppens, Bell and Chakraborty used KMC to calculate the loading dependence of self diffusion for a variety of lattices, for comparison with mean field theories (MFT) of diffusion.[122] These theories usually predict $D_s(\theta) \cong D_0(1 - \theta)$, where θ is the fractional occupancy of the lattice and D_0 is the self diffusivity at infinite dilution. Coppens *et al.* found that the error incurred by MFT is greatest for lattices with low coordination numbers, such as silicalite and other MFI-type zeolites. Coppens *et al.* then reported KMC simulations showing that by varying the concentrations of weak and strong binding sites (*cf.* S_{II} and W sites), their system exhibits most of the loading dependencies of self diffusion reported by Kärger and Pfeifer.[123]

In all these studies, the jump frequencies and reaction rate coefficients were estimated in various *ad hoc* ways. In contrast, Trout, Chakraborty and Bell applied electronic structure methods to calculate thermodynamic parameters for possible elementary reactions in the decomposition of NO_x over Cu-ZSM-5.[124] Based on these insights, they developed a KMC model of reaction and diffusion in this system, seeking the optimal distribution of isolated reactive Cu centers.[125] This hierarchical approach to realistic modeling of complex systems presents an attractive avenue for future research.

Auerbach and co-workers have reported a series of studies modeling the concentration dependence of benzene diffusion in Na-X and Na-Y zeolites,[21,22,24,25,31] because of persistent, qualitative discrepancies between different experimental probes of the coverage dependence of self diffusion.[7] PFG NMR diffusivities decrease monotonically with loading for benzene in Na-X,[111] while tracer zero-length column (TZLC) data *increase* monotonically with loading for the same system.[126] TZLC is a flow method that measures the desorption rate arising from tracer exchange in a zero-length chromatographic column containing zeolite particles. The TZLC data is converted to self diffusivities through a model assuming that tracer exchange introduces no chemical potential gradient. PFG NMR differs from TZLC in that the NMR experiment directly measures the mean square displacement of magnetically labeled particles at equilibrium in a zeolite.

Addressing this discrepancy between PFG NMR and TZLC with theory and simulation may provide better understanding of the microscopic physics essential to benzene transport

in Na-X and Na-Y. In addition, by varying fundamental energy scales, our model for these systems exhibits four of the five loading dependencies of self diffusion reported by Kärger and Pfeifer,[123] in analogy with the study of Coppens *et al.*[127] However, because the critical temperature of bulk benzene is over 560 K, attractive guest–guest interactions are significant and should not be ignored. Modeling such systems remains challenging because of the coupling between rare event dynamics and strong guest–guest interactions,[26,128] i.e. the competition between adhesive and cohesive forces. In what follows, we outline our recently developed model for determining how guest–guest interactions modify activation energies of site-to-site jumps.[25,31] Based on this model, our calculations for benzene in Na-X described below give excellent qualitative agreement with PFG NMR diffusivities, and give qualitative disagreement with TZLC data.

It should not be surprising that this three-dimensional lattice model of benzene in Na-X with attractive interactions supports phase transitions from low to high sorbate density, analogous to vapor–liquid equilibrium of bulk benzene.[28] We examine this phase transition below, using grand canonical lattice Monte Carlo and thermodynamic integration to explore the nature of subcritical and supercritical phases. We also explore the impact of this phase transition on diffusion in zeolites. In general, we find that understanding the thermodynamics of confined fluids can be crucial for elucidating the transport properties of molecules in zeolites.[129,130]

A. Supercritical Diffusion: Theory and Simulation

Thus far we have discussed the dynamics and diffusion of benzene in Na-Y; we now turn our attention to benzene in Na-X. As discussed in the Introduction, Na-X is a FAU-type zeolite with Si:Al ratios in the range 1.0–1.5, and hence with a higher density of Na cations than that in Na-Y. Locating benzene adsorption sites in Na-X is more difficult because of these additional Na cations, which lie in or near the 12-ring window separating adjacent supercages.[52,131] The powder neutron diffraction study of Vitale *et al.*[52] found benzene in Na-X only at S_{II}, but located only half the adsorbed benzene, suggesting that low-symmetry benzene sites near the 12-ring window are likely. These binding sites would act as intermediates for cage-to-cage motion, in analogy with Na-Y W sites. As such, we denote benzene sites near Na cations in 12-ring windows as Na-X W sites, although strictly speaking their geometries and energies differ from those of Na-Y W sites. In particular, we expect that Na-X W sites are stabilized relative to those in Na-Y, because of these additional Na cations in Na-X. The lattice of benzene binding sites in Na-X and Na-Y thus contains four tetrahedrally arranged S_{II} sites and four tetrahedrally arranged, doubly shared W sites per supercage. Saturation coverages of *ca.* 6 molecules per cage are found for benzene in Na-X and Na-Y,[69] corresponding to occupation of all S_{II} and W sites. In equations that follow, the W and S_{II} sites are denoted sites 1 and 2, respectively.

1. Parabolic Jump Model

A lattice gas model is used to describe the thermodynamics of these systems, limiting the range of guest–guest interactions to nearest neighbors. The Hamiltonian for a lattice

with M_1 W sites and $M_2 = 2M_1 = M - M_1$ S$_{\text{II}}$ sites, takes the form:

$$H(\vec{s}, \vec{\sigma}) = \sum_{i=1}^{M_1} s_i f_1 + \frac{1}{2} \sum_{i,j=1}^{M_1} s_i J_{ij}^{11} s_j + \sum_{i=1}^{M_1} \sum_{j=1}^{M_2} s_i J_{ij}^{12} \sigma_j + \frac{1}{2} \sum_{i,j=1}^{M_2} \sigma_i J_{ij}^{22} \sigma_j + \sum_{i=1}^{M_2} \sigma_i f_2 \qquad (3.1)$$

where $\vec{s}$ and $\vec{\sigma}$ are site occupation numbers for W and S$_{\text{II}}$ sites, respectively, and f_1 and f_2 are their respective site free energies given by $f_i = \varepsilon_i - T s_i$. In Eq. (3.1), J_{ij}^{11}, J_{ij}^{12} and J_{ij}^{22} are the nearest neighbor W–W, W–S$_{\text{II}}$ and S$_{\text{II}}$–S$_{\text{II}}$ interactions, respectively, i.e. $J_{ij}^{11} = J_{11}$ for nearest neighbor W sites and zero otherwise, and so on for J_{ij}^{12} and J_{ij}^{22}. These parameters are obtained from the second virial coefficient of the heat of adsorption,[69,132] yielding *ca.* $J = J_{12} = J_{22} \cong -4$ kJ mol^{-1}. However, to determine qualitatively how guest–guest interactions control the loading dependence of the self diffusivity, we vary J_{12} and J_{22} over the range 0 to -10 kJ mol^{-1}.

The site binding energies are taken as $\varepsilon_2 = -78$ kJ mol^{-1} and $\varepsilon_1 = -63$ kJ mol^{-1} for benzene in Na-X, and $\varepsilon_2 = -78$ kJ mol^{-1} and $\varepsilon_1 = -53$ kJ mol^{-1} for benzene in Na-Y.[25,31] Site 2 is chosen for the zero of entropy in both Na-X and Na-Y, giving $s_2 \equiv 0$. Given the data in Table II, the entropy for site 1 is therefore $s_1 = k_B \ln(7.1) = 1.96 k_B$. The results we find below are particularly sensitive to the parameter $(f_1 - f_2)/|J|$, of which f_1 is the most poorly known. This fact underscores the importance of obtaining more precise structural information for the Na-X W site, perhaps by synthesizing larger Na-X crystals to facilitate single-crystal diffraction studies.[131]

We may be tempted to use the rate data in Table II to parameterize our model at infinite dilution. However, since the diffusivity is especially sensitive to activation energies, we must recognize that our calculated barriers may not be the most accurate of all available data. We choose instead to extract activation energies from experimental data for benzene in Na-X[17,111] and Na-Y,[17,66] yielding the barriers below in Table III. We do utilize the Arrhenius pre-exponential factors in Table II for benzene in Na-Y, and assume that they also hold for benzene in Na-X.

	Na-Y	Na-X
S$_{\text{II}} \to$ S$_{\text{II}}$	25	15
S$_{\text{II}} \to$ W	38	25
W $\to$ S$_{\text{II}}$	13	10
W $\to$ W	13	10

Table III. Best available activation energies (kJ mol^{-1}) for benzene jumps at infinite dilution in Na-X and Na-Y.

The attractive guest–guest interactions introduce new complexities into the kinetics of the diffusion problem, as discussed above. An extreme case of this was recently reported by Sholl and Fichthorn,[115] wherein strong guest–guest interactions generated transport dominated by correlated cluster dynamics instead of single molecule jumps. While such correlated clusters are not likely to dominate benzene diffusion in FAU-type zeolites, guest–guest interactions will modify jump activation energies for site-to-site rate coefficients, depending

upon specific configurations of neighboring adsorbates. In order to account for this, we have generalized a model that relates binding energies to transition state energies used previously by Hood *et al.*,[133] and also used by us for predicting mobilities in zeolites.[17] To implement this approach, it is convenient to write the lattice gas Hamiltonian in the following form:

$$H(\vec{n}) = \sum_{i=1}^{M} n_i \tilde{f}_i + \frac{1}{2} \sum_{i,j=1}^{M} n_i \tilde{J}_{ij} n_j, \tag{3.2}$$

where $\vec{n} = (n_1, n_2, \cdots, n_M)$ are site occupation numbers listing a configuration of the system, and $\tilde{f}_i = \tilde{\varepsilon}_i - T\tilde{s}_i$ is the free energy for binding in site i. In Eq. (3.2), $\tilde{J}_{ij}$ is the nearest neighbor interaction between sites i and j, i.e. $\tilde{J}_{ij} = 0$ if sites i and j are not nearest neighbors.

We assume that the minimum energy hopping path connecting adjacent sorption sites is characterized by intersecting parabolas, shown in Fig. 8, with the site-to-site transition state located at the intersection point. For a jump from site i to site j, with $i, j = 1, \ldots, M$, the hopping activation energy including guest–guest interactions is given by:

$$E_a(i,j) = E_a^{(0)}(i,j) + \Delta E_{ij} \left(\frac{1}{2} + \frac{\delta E_{ij}^{(0)}}{k_{ij} a_{ij}^2} \right) + \Delta E_{ij}^2 \left(\frac{1}{2 k_{ij} a_{ij}^2} \right), \tag{3.3}$$

where $E_a^{(0)}(i,j)$ is the activation energy without guest–guest interactions, i.e. the infinite dilution activation energy, and a_{ij} is the jump distance. ΔE_{ij} is the *shift* in the energy difference between sites i and j resulting from guest–guest interactions, and is given by $\Delta E_{ij} = \delta E_{ij} - \delta E_{ij}^{(0)} = (E_j - E_i) - (\tilde{\varepsilon}_j - \tilde{\varepsilon}_i)$, where $E_k = \tilde{\varepsilon}_k + \sum_{l=1}^{M} \tilde{J}_{kl} n_l$ for a particular lattice configuration $\vec{n}$. This method allows the rapid estimation of configuration dependent barriers during a KMC simulation, knowing only infinite dilution barriers and the nearest neighbor interactions defined above. The parabolic jump model is most accurate when the spatial paths of jumping molecules are not drastically changed by guest–guest interactions, although the energies can change as shown in Fig. 8. While other lattice models of diffusion in zeolites have been proposed that account for attractive guest–guest interactions,[26,128] the parabolic jump model has the virtue of being amenable to analytical solution, as discussed next.
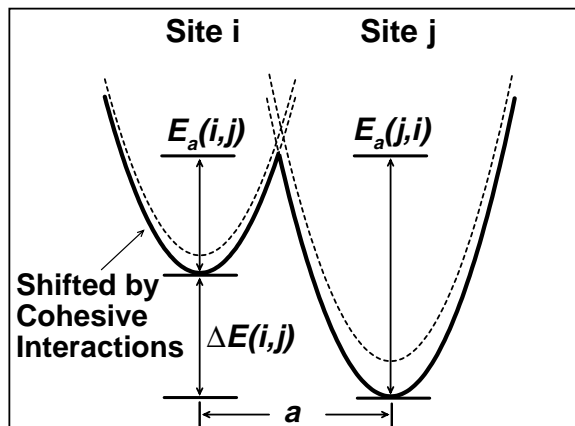

Figure 8. Site-to-site jump activation energies perturbed by guest–guest interactions, approximated with parabolic jump model.

2. Mean Field Theory

Mean field theory (MFT) provides a powerful means of reducing the complexity of many-body structure and dynamics to the simplicity of effective one-body properties.[39] MFT averages over local fluctuations in the instantaneous energy of each adsorption site, thereby neglecting correlations that extend beyond the length scale separating sites. Although MFT can give numerical error for lattices with low coordination,[122] the theory remains qualitatively reliable except near critical points, where cooperativity in fluctuations extends over large distances. Thus, we view MFT as a useful launching point for an analytical theory of many-body diffusion in zeolites. We note that a general theoretical method called dynamical MFT has recently been reported,[134] which is reminiscent of our approach outlined below.

We have shown that a mean field analysis applied to cage-to-cage motion through Na-X and Na-Y yields $D_s(\theta) \cong \frac{1}{6}k_\theta a_\theta^2$, where a_θ is the mean intercage jump length, and $1/k_\theta$ is the mean cage residence time.[21] The mean cage-to-cage jump distance has a very weak temperature and loading dependence,[24] remaining in the range 11–13 Å as dictated by the Na-X supercage structure. We have also shown[21] that the cage-to-cage rate coefficient, k_θ, is given by $k_\theta = \kappa \cdot k_1 \cdot P_1$, where P_1 is the probability of occupying a W site, k_1 is the total rate of leaving a W site, and κ is the transmission coefficient for cage-to-cage motion. This theory provides a picture of cage-to-cage motion involving transition state theory ($k_1 \cdot P_1$) with dynamical corrections (κ), which is valid for both weak *and* relatively strong guest–guest interactions. For consistency with our mean field analysis, we assume that $\kappa = \frac{1}{2}$ for all loadings. We also expect that P_1 will increase with loading, and that k_1 will decrease with loading. Below we outline the derivation of analytical expressions for k_1 and P_1, to elucidate how the balance between k_1 and P_1 controls the loading dependence of self diffusion.[25,31]

In the Na-X and Na-Y lattices, with twice as many S_{II} sites as W sites, P_1 is given by $1/(1 + 2\theta_2/\theta_1)$, where θ_1 and θ_2 are the fractional coverages on W and S_{II} sites, respectively. We determine θ_1 and θ_2 in the grand canonical ensemble, according to:

$$\theta_1 \cong \langle s_i \rangle_{MF} = \frac{e^{-\beta[(f_1-\mu)+6(J_{11}\theta_1+J_{12}\theta_2)]}}{1 + e^{-\beta[(f_1-\mu)+6(J_{11}\theta_1+J_{12}\theta_2)]}} \tag{3.4}$$

$$\theta_2 \cong \langle \sigma_i \rangle_{MF} = \frac{e^{-\beta[(f_2-\mu)+3(J_{22}\theta_2+J_{12}\theta_1)]}}{1 + e^{-\beta[(f_2-\mu)+3(J_{22}\theta_2+J_{12}\theta_1)]}}, \tag{3.5}$$

where μ is the chemical potential and $\beta = (k_B T)^{-1}$. The factors of 3 and 6 in Eqs. (3.4) and (3.5) arise from the site connectivity among S_{II} and W sites. The total fractional coverage is then given by $\theta = (\theta_1 + 2\theta_2)/3$.

The MFT expression for the loading dependence of k_1, the total rate of leaving a W site, is given by:

$$k_1 \cong 6(1 - \theta_1)\langle k_{1\to1}\rangle + 6(1 - \theta_2)\langle k_{1\to2}\rangle, \tag{3.6}$$

where $6(1 - \theta_j)$ counts available target sites, and $\langle k_{1\to j}\rangle$ averages over fluctuating rate coefficients for jumps leaving W sites. As described above, we model the fluctuating activation energies according to the parabolic jump model. Assuming that fluctuations in the pre-exponentials can be ignored and that activation energies are Gaussian-distributed, we have that:

$$\langle k_{i \to j} \rangle \cong \nu_{i \to j} \langle e^{-\beta E_a(i,j)} \rangle$$
$$= \nu_{i \to j} \cdot e^{-\beta \langle E_a(i,j) \rangle} \cdot e^{-\beta^2 \sigma_a^2(i,j)/2}, \tag{3.7}$$

where $\sigma_a^2(i,j)$ is the variance of the Gaussian distribution of activation energies, i.e. $\sigma_a^2(i,j)$ $= \langle [E_a(i,j) - \langle E_a(i,j) \rangle]^2 \rangle = \langle [E_a(i,j)]^2 \rangle - \langle E_a(i,j) \rangle^2$. We see from Eq. (3.3) that applying mean field theory requires averages of ΔE_{ij}^k up to $k = 4$. We only consider terms up to second order, since higher order terms will typically be small.

3. Comparison with Simulation and Experiment

To test the accuracy of this MFT, we used KMC and the parabolic barrier model to calculate benzene mean square displacements in Na-X.[31] Figure 9 shows that three "diffusion isotherm" types emerge. We see in Fig. 9 excellent qualitative agreement between theory (lines) and simulation (dots). MFT consistently overestimates simulated diffusivities because theory neglects correlations that increase the probability of the particle returning to its original position. These diffusion isotherm types differ in the coverage that gives the maximum diffusivity: $\theta_{\max} = 0$ is defined as type I, $\theta_{\max} \in (0, 0.5]$ is type II, and $\theta_{\max} \in (0.5, 1]$ is type III. Defining the parameter $\chi \equiv (f_1 - f_2)/k_B T$, we find that type I typically arises from $\chi < 1$, type II from $\chi \sim 1$, and type III from $\chi > 1$. This suggests that when the S_{II} and W sites are nearly degenerate, i.e. $\chi \lesssim 1$, the coverage dependence of P_1 is weak, and hence k_θ and $D_s(\theta)$ are dominated by the decreasing coverage dependence of k_1. Alternatively, when $\chi \gtrsim 1$, the enhancement of P_1 at higher loadings dominates the diffusivity until $\theta_1 \sim \theta_2$, at which point the decreasing k_1 begins to dominate.[127] We also obtain excellent qualitative agreement between theory and simulation for the temperature dependence of diffusion for all cases studied.[31]
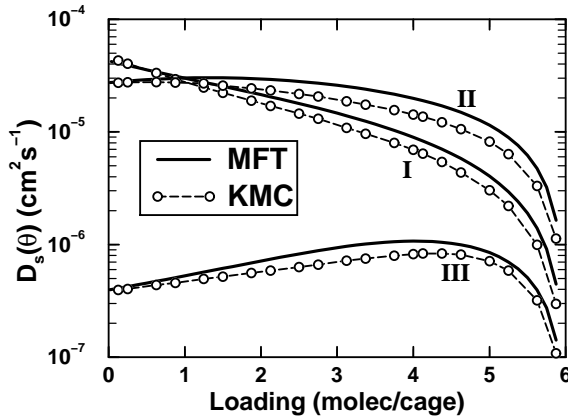

Figure 9. Comparison between KMC and MFT for benzene in Na-X at three different temperatures, showing that three diffusion isotherm types emerge.

Figure 10 shows KMC calculated diffusion isotherms for benzene in Na-X at $T = 393$ K and 468 K, compared to PFG NMR data[111] at the same temperatures (uniformly scaled by a factor of 5), and TZLC diffusivities[126] at $T = 468$ K (uniformly scaled by a factor of 100). The experimental data were scaled to facilitate comparison with the loading dependence

predicted by simulation, which itself was *not* fitted to either experimental result. Figure 10 shows that our model is in excellent qualitative agreement with the PFG NMR results, and in qualitative disagreement with TZLC. Other experimental methods yield results that also agree broadly with these PFG NMR diffusivities.[135−137] Our model overestimates PFG NMR diffusivities at high loadings because the lattice model allows 6 molecules per cage, while the observed saturation coverage is 5.4 molecules per cage.
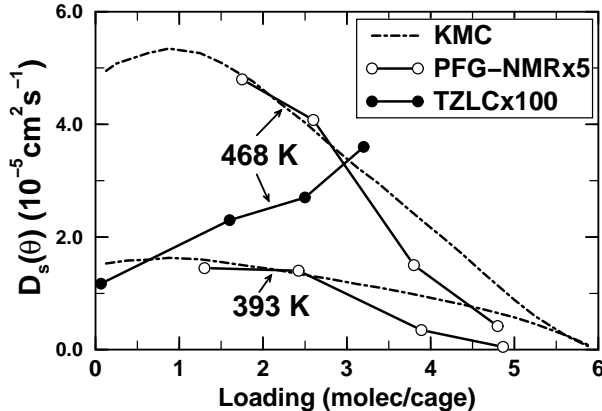
Figure 10. Diffusion isotherm for benzene in Na-X at 468 K, by PFG NMR (scaled by 5), TZLC (scaled by 100) and by KMC simulations.

One way to view the discrepancy in Fig. 10, apart from the absolute magnitudes, is that both simulation and PFG NMR are consistent with a low coverage of maximum diffusivity, θ_{max}, while TZLC exhibits a large θ_{max}. While it is not obvious why the TZLC results differ so markedly from PFG NMR data and from our simulated diffusivities, our results in Ref. 31 do suggest future experiments to test the reliability of TZLC. Indeed, we found in Ref. 31 that θ_{max} decreases with increasing temperature, as all sites become more degenerate. As such, high temperature TZLC diffusion isotherms should be measured, to confirm consistency with our rather plausible prediction regarding the temperature dependence of θ_{max}.

Buoyed by the apparent success of our transport theory, we now ask the question: can this system undergo a phase transition analogous to vapor–liquid equilibrium of bulk benzene, driven by the attractive nearest neighbor interactions in our model? Clearly we cannot distinguish between "vapor" and "liquid" inside an individual zeolite cage, but effective cage-to-cage attractions may lead to cooperativity on longer length scales. Traditionally, the fields of transport and adsorption in zeolites have enjoyed little overlap.[129,130] In the Secs. III B and III C, we attempt to connect these two fields for benzene in Na-X and Na-Y.

B. Vapor–Liquid Equilibrium

The thermodynamic properties of confined fluids play a central role in separations and reactions that take place within porous materials.[138,139] Of particular interest are hysteresis loops and precipitous jumps in adsorption isotherms, since these are often associated with

vapor–liquid transitions of the confined fluid. Although there is a vast literature on such transitions in mesoporous materials, there are very few reports of phase transitions in microporous solids such as zeolites. This is presumably because confinement into such small cavities (< 20 Å) reduces the vapor–liquid critical temperature to extremely low values.

Nevertheless, there have been occasional reports of possible phase transitions in such systems. For example, hysteresis loops have been observed at 77 K for methane in AlPO$_4$-5,[140] a one-dimensional channel zeolite. Since phase transitions in one-dimensional systems are theoretically forbidden,[39] Radhakrishnan and Gubbins[141] and Maris *et al.*[142] simulated this system to determine whether interactions among methanes in adjacent channels could account for the observed phase transition. They found critical temperatures of 52 K and 33 K, respectively, arising from different levels of detail in their models of AlPO$_4$-5. For benzene in Na-Y, a multiple-quantum proton NMR study detected a continuous network of coupled proton spins,[143] suggesting the importance of interactions among molecules in adjacent cages. We have used grand canonical Monte Carlo[46] (GCMC) and thermodynamic integration[94,144,145] to demonstrate that these cooperative interactions can lead to vapor–liquid transitions for benzene in Na-X.[28]

1. Adsorption Isotherms and Coexistence Curves

In GCMC simulations, the chemical potential μ, volume V, and temperature T are fixed, while the number of adsorbed molecules is allowed to fluctuate. We have performed Metropolis GCMC calculations on a simulation cell that consists of eight Na-X unit cells, containing 128 W sites and 256 S$_{II}$ sites. The lattice model is parameterized as discussed in Sec. III A, using $J = J_{12} = J_{22} = -0.04$ eV $= -3.86$ kJ mol^{-1}. The average fractional occupancy is calculated after $(1.0 - 2.5) \times 10^7$ Monte Carlo (MC) steps, with an initial equilibration period of 10^6 MC steps. The GCMC isotherms are calculated over a grid of $\mu^* = (\mu - \varepsilon_2)/|J|$. In the deep subcritical regime we observe hysteresis between the GCMC calculations performed by adsorbing molecules onto an empty lattice, *viz.* the adsorption or vapor branch; and desorbing molecules from a fully occupied lattice, *viz.* the desorption or liquid branch. For higher temperatures in the subcritical region, greater than 300 K ($T^* = k_B T/|J| = 0.65$), the hysteresis region becomes too narrow to be recovered from GCMC adsorption and desorption calculations. The liquid and vapor branches for these temperatures are obtained by averaging separately the vapor and liquid densities that arise from a single GCMC run. The liquid and vapor branches are used for performing thermodynamic integration,[28,94,144,145] which leads to the vapor–liquid coexistence curve.

It is not possible to approach the critical point very closely using the Metropolis algorithm, because this algorithm does not efficiently produce the macroscopic fluctuations that characterize the critical point. More sophisticated algorithms have been developed that create and destroy large clusters, rather than individual particles, thereby simulating large density fluctuations efficiently.[146−148] In order to obtain an estimate of the critical point from Metropolis simulations, we fitted the coexistence points to the Ising scaling law for the density difference between the liquid and vapor phases for three-dimensional systems, i.e. $(T_c - T) = A(\rho_l - \rho_g)^3$, together with the law of rectilinear diameters.[141,149] We also estimate the critical point with MFT, using Eqs. (3.4) and (3.5) to calculate adsorption isotherms.

We have performed GCMC adsorption and desorption calculations for benzene in Na-X over the temperature range 50–700 K. For $T > 400$ K ($T^* = 0.86$), the isotherms are continuous and reversible with respect to the adsorption and desorption branches. However, for lower temperatures, regions of hysteresis are observed because of metastabilty in the adsorbed state. In Fig. 11, we show the hysteresis region that arises at $T = 340$ K ($T^* = 0.73$). This hysteresis region is extremely narrow, with a width of only $0.02|J|$. This phase transition occurs because of attractive interactions between benzene molecules in adjacent cages. These interactions are mediated by benzene molecules in W sites, which are shared between adjacent supercages, and hence are able to build a continuous network of coupled benzenes.
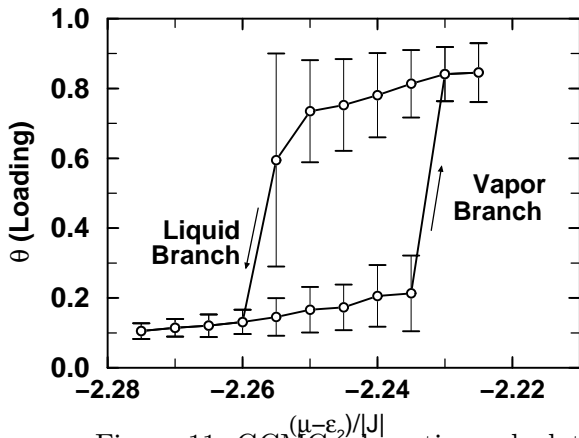
Figure 11. GCMC adsorption calculation for benzene in Na-X, showing hysteresis at $T = 340$ K ($T^* = 0.73$).
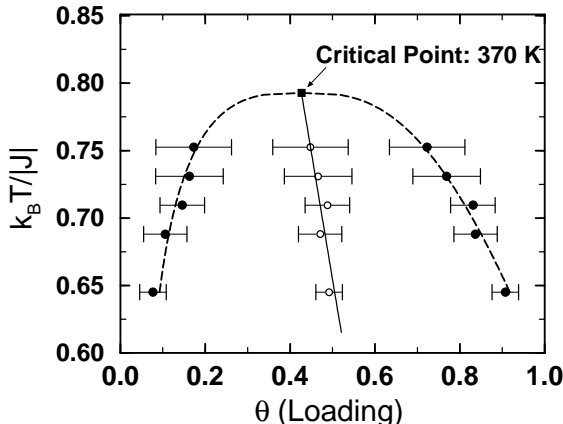
Figure 12. Simulated coexistence envelope for benzene in Na-X, giving $T_c = 370 \pm 20$ K ($T_c^* = 0.79 \pm 0.04$).

The coexistence envelope for benzene in Na-X obtained from thermodynamic integration is shown in Fig. 12. The asymmetry in the coexistence curve arises from the presence of two different types of sites in our model. The critical point we estimate for benzene in Na-X is $T_c = 370 \pm 20$ K ($T_c^* = 0.79 \pm 0.04$) and $\theta_c = 0.45 \pm 0.05$. Applying the same analysis to adsorption isotherms obtained with MFT, we obtain a mean field critical temperature of 691 K ($T_c^*(\text{MFT}) = 1.48$). We thus find that MFT greatly over estimates the critical temperature for this lattice model, hence requiring the GCMC simulations.

It is interesting to compare the reduced critical temperature found above to those from other lattices, in order to understand what aspects of our lattice model for benzene in Na-X determine its critical point. In particular, each actual site interacts with 6 nearest neighbors, while the overall tetrahedral symmetry of FAU-type zeolites provides 4 direct cage-to-cage interactions. It is not obvious, then, whether the critical point for benzene in Na-X should be characteristic of lattices with 4-fold or 6-fold coordination. T_c^* for the 2-d square lattice is 0.58, while that for the 3-d cubic lattice is 1.0.[39] Our system, with $T_c^* = 0.79$, happens to fall right in between the results for these two lattices, suggesting that the interplay between local coordination and cage-to-cage couplings controls the critical point for benzene in Na-X. This analysis also suggests why MFT, which is only sensitive to local coordination as shown in Eqs. (3.4) and (3.5), so grossly overestimates the critical temperature.

29

The existence of this phase transition is sensitive to the value of the parameter $\gamma \equiv (f_1 - f_2)/|J|$. If γ exceeds a certain value, the critical temperature vanishes along with the phase transition. Preliminary calculations show that when $\gamma \gtrsim 4$, which is the case for benzene in Na-Y, the phase transition is completely suppressed. Indeed, without entropy favoring benzene W sites, the phase transition would also be suppressed in our model of benzene in Na-X. This sensitivity underscores yet again the importance of obtaining more precise structural information for the Na-X W site, to quantify f_1 more accurately. Although hysteresis has been observed in adsorption isotherms measured for benzene in Na-X,[150] this observation must arise from a structural transformation of the zeolite rather than from cooperative interactions among guests, because the measured densities in the adsorption branch *exceed* those in the desorption branch. As such, our predictions for benzene in Na-X await experimental confirmation.

Our analysis above suggests that this phase transition should be even more pronounced for benzene in Si-Y, where zeolite–benzene interactions are weaker than they are in Na-X. Performing off-lattice GCMC simulations on benzene in Si-Y thus constitutes an important avenue for future research. These calculations will likely require configurational-bias Monte Carlo[151,152] to facilitate inserting anisotropic adsorbates at high density.

Based on these thermodynamic studies, we now understand that the diffusion isotherms compared with experiment in Fig. 10 represent supercritical lattice gas diffusion—hence the name of Sec. III A—because these simulations were performed at temperatures above $T_c = 370$ K. It is irresistible to wonder how transport in zeolites becomes modified when considering *subcritical* lattice gas diffusion.

C. Subcritical Diffusion: Droplet Formation

The comprehensive loading dependence of diffusion in these systems is controlled by the degree of degeneracy between S_{II} and W sites, which depends upon three energy scales: $f_1 - f_2$, J and $k_B T$. As such, two unitless parameters are required to describe the Corresponding States of benzene in Na-X and Na-Y. It is convenient now to utilize the parameter $T^* = k_B T/|J|$. This Corresponding States parameter suggests that benzene becomes a subcritical fluid in Na-X by either decreasing T or increasing $|J|$. For computational convenience we prefer to increase $|J|$, which allows us to compare diffusion isotherms at fixed temperature.

Figure 13 shows KMC calculated diffusion isotherms for benzene in Na-X at 468 K, using various values of the coupling parameter J.[31] These diffusion isotherms were calculated from mean square displacements (KMC-MSD), and also were estimated from the mean field approximation (KMC-MFA): $D_s(\theta) \cong \frac{1}{6} k_\theta a_\theta^2$, where k_θ and a_θ are determined from KMC simulations. These two methods agree semi-quantitatively as shown in Fig. 13, which simplifies KMC simulations because k_θ and a_θ are time-independent quantities, in contrast to mean square displacements whose time-dependence must be calculated. The thermodynamic analysis above indicates that the diffusion isotherms in Fig. 13 using $|J| \leq 0.04$ eV represent supercritical diffusion. The loading dependence exhibited by these isotherms is weakly type II, and qualitatively demonstrates the monotonically decreasing $(1 - \theta)$ form predicted by simple MFT. In related calculations, we find a type III diffusion isotherm for supercritical benzene in Na-Y, which arises because W sites in Na-Y are relatively unstable

at most temperatures. In general, we find that increasing temperature and/or making J more negative, while keeping all other parameters constant, changes isotherms according to type III → II → I.
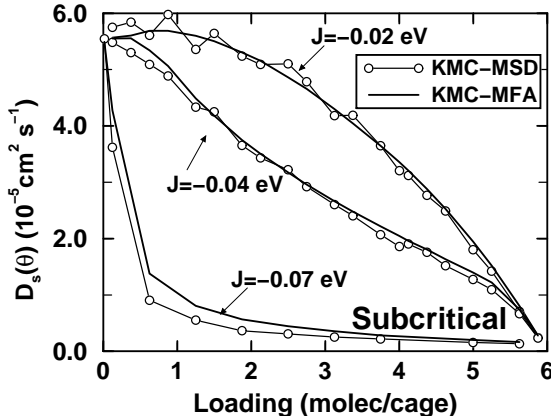

Figure 13. Diffusion isotherms for benzene in Na-X by KMC-MSD and KMC-MFA (see text) at 468 K for various values of J, showing the signature of subcritical diffusion for $J = -0.07$ eV.

On the other hand, when $J = -0.07$ eV we find an interesting loading dependence, involving a sharp decrease for small loadings, followed by a broad region of constant diffusivity for higher loadings. If we assume for the moment that $T_c \propto |J|$, then $T_c \approx 650$ K in Na-X with $J = -0.07$ eV. Since the self diffusivities in Fig. 13 were calculated at 468 K, the simulations using $J = -0.07$ eV represent *subcritical* diffusion. Since canonical KMC simulations fix the loading, a subcritical system at, e.g., $\theta = 0.5$ will involve a fluctuating liquid-like cluster of filled sites occupying approximately half the lattice, while a supercritical system at the same loading will be more evenly dispersed throughout the lattice, as shown schematically in Fig. 14. This insight explains our intriguing simulation results, and may help elucidate experimental findings as well. In particular, cluster formation in subcritical systems suggests a diffusion mechanism involving "evaporation" of particles from clusters. Increasing the loading in subcritical systems increases mean cluster sizes, and smoothes cluster interfaces. Once these interfaces become sufficiently smooth, we can assume that evaporation dynamics remain essentially unchanged by further increases in loading. As such, we expect the subcritical diffusivity to obtain its full loading value at low loadings, and then remain roughly constant up to full loading, as shown for Na-X in Fig. 13.
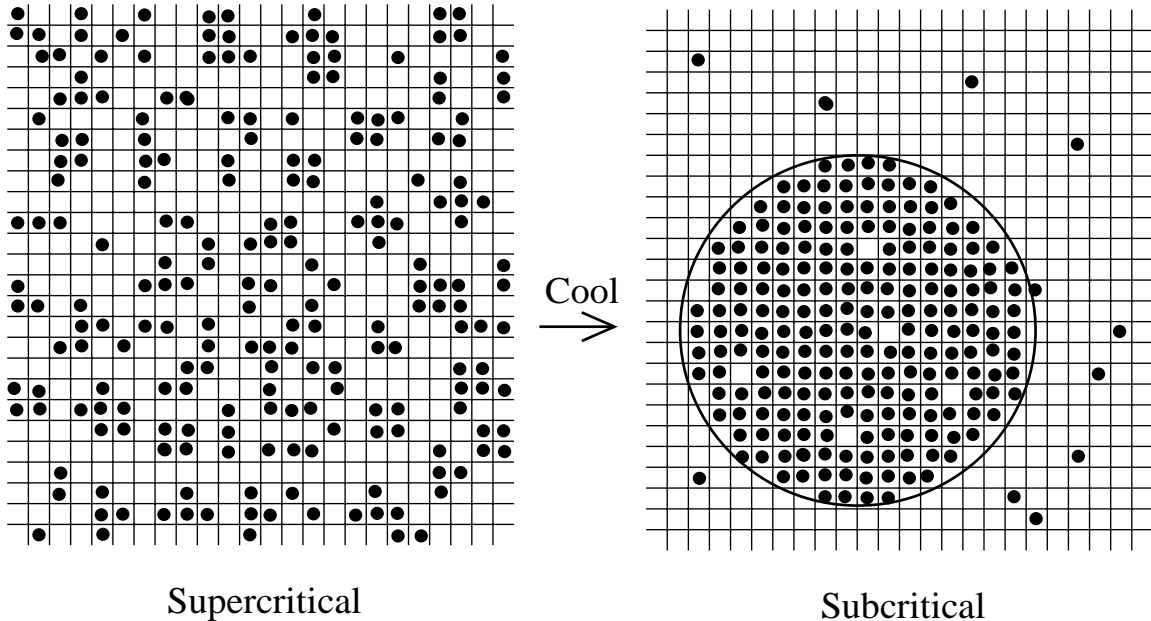
31

Figure 14. Schematic of cluster formation in subcritical nanoporous systems, where the subcritical droplet spans many Na-X cages that are full of benzene.

This subcritical type of loading dependence, involving broad regions of constant diffusivity, is surprising because isotherms for interacting adsorbates are expected to decrease with loading when site blocking dominates. It is interesting to note that an isotherm type has been reported for strongly associating adsorbates such as water and ammonia,[123] denoted by Kärger and Pfeifer as type III (not to be confused with our type III), involving an initial increase followed by a broad region of constant diffusivity. The present analysis suggests that Kärger and Pfeifer's type III diffusion isotherm may be characteristic of a cluster-forming, subcritical adsorbed phase.

Thus far we have focused on equilibrium transport processes such as self diffusion and orientational randomization. We now turn our attention to modeling non-equilibrium diffusion in nanopores, which is the process most relevant to industrial applications.

IV. NONEQUILIBRIUM DIFFUSION IN NANOPORES

Two theoretical formulations exist for modeling non-equilibrium diffusion, hereafter denoted "transport diffusion," which ultimately arises from a chemical potential gradient or similar driving force.[7,8] The formulation developed by Fick involves linear response theory relating macroscopic particle flows to concentration gradients, according to $J = -D\nabla\theta$, where J is the net particle flux through a surface $\mathcal{S}$, D is the transport diffusivity, and $\nabla\theta$ is the local concentration gradient perpendicular to the surface $\mathcal{S}$.[39] While this perspective is conceptually simple, it breaks down qualitatively in remarkably simple cases, such as a closed system consisting of a liquid in contact with its equilibrium vapor. In this case, Fick's law would predict a non-zero macroscopic flux; none exists because the chemical potential gradient vanishes at equilibrium. Fick's law can be generalized to treat very simple multi-component systems,[29,30,153−156] such as co-diffusion and counter-diffusion of identical, tagged particles.

Despite these shortcomings, Fick's law remains the most natural formulation for transport diffusion through Langmuirian lattice models of zeolite–guest systems. These involve regular lattices of identical sorption sites where guest–guest interactions are ignored, except for exclusion of multiple site occupancy. Such model systems exhibit Langmuir adsorption isotherms, and give single-component transport diffusivities that are independent of loading.[157] Moreover, for such systems the equation $J = -D\nabla\theta$ is exact for all concentration gradients, i.e. all higher order terms beyond linear response theory cancel. We exploit this fact below in our lattice model studies of counter-permeation through anisotropic[29] and single-file nanoporous membranes.[30]

The other formulation of transport diffusion was developed independently by Maxwell and Stefan, and begins with the equation $J = -L\nabla\mu$, where L is the so-called Onsager coefficient and $\nabla\mu$ is a local chemical potential gradient at the surface $\mathcal{S}$.[7,158] To make contact with other diffusion theories, the Onsager coefficient is written in terms of the so-called corrected diffusivity, D_c, according to $L = \theta D_\mathrm{c}/k_B T$, where θ is the local intracrystalline loading at the surface $\mathcal{S}$. Clearly this formulation does not suffer from the qualitative shortcomings of Fick's law, and can be properly generalized for complex multicomponent systems.[159] The corrected diffusivity depends upon loading for Langmuirian systems, where jump diffusion holds, but depends very weakly on loading for more fluid-like diffusion systems,[158] making the Maxwell-Stefan formulation more natural for weakly binding zeolite–guest systems. The relationship between the Fickian and Maxwell-Stefan diffusivities is often called the Darken equation, given by:[7]

$$D = D_\mathrm{c} \left(\frac{\partial \ln f}{\partial \ln \theta} \right)_T, \tag{4.1}$$

where f is the fugacity of the external fluid phase. Other versions of the Darken equation often appear, e.g., where D_c is replaced with D_s, the self diffusivity. We find for Langmuirian systems that this replacement is tantamount to mean field theory (MFT).[29]

Many researchers prefer to report their transport data in terms of the corrected diffusivity because it is completely determined by dynamics, in contrast to the Fickian diffusivity which is also influenced by thermodynamics, as evidenced by the adsorption factor in Eq. (4.1). Indeed, a correlation function analysis of the corrected diffusivity yields:[36,158,160]

$$D_\mathrm{c} = \frac{1}{3N} \sum_{i,j=1}^{N} \int_0^\infty dt \, \langle \vec{v}_i(0) \cdot \vec{v}_j(t) \rangle \tag{4.2}$$

$$= \frac{1}{3N} \sum_{i,j=1}^{N} \lim_{t\to\infty} \frac{1}{2t} \langle \delta\vec{r}_i(t) \cdot \delta\vec{r}_j(t) \rangle, \tag{4.3}$$

where N is the number of particles in the system, and $\vec{v}_i(t)$ and $\delta\vec{r}_i(t) = \vec{r}_i(t) - \vec{r}_i(0)$ are the velocity and displacement of the ith particle at time t, respectively. Both Eqs. (4.2) and (4.3) can be used for fluid-like diffusion, e.g. for methane in silicalite, while only Eq. (4.3) is convenient for jump diffusion, e.g. for benzene in Na-Y, because velocity correlations typically decay well before rare jump events occur. The interparticle correlation functions in Eqs. (4.2) and (4.3) manifest the collective nature of non-equilibrium diffusion, which is why this type of transport is often called collective diffusion. The correlation functions in Eqs.

(4.2) and (4.3) also suggest that non-equilibrium diffusion can be modeled with equilibrium simulations *viz.* the fluctuation-dissipation theorem,[39] though the poor statistics of such simulations make them very challenging. An interesting avenue for future research involves the use of Eq. (4.3) with realistic lattice models,[161] to develop a feasible equilibrium approach for modeling non-equilibrium diffusion in zeolites.

In the limit of low loading, interparticle correlations vanish and Eqs. (4.2) and (4.3) become:

$$D_{\rm c} \xrightarrow{\theta \to 0} \frac{1}{3N} \sum_{i=1}^{N} \int_0^\infty dt \, \langle \vec{v}_i(0) \cdot \vec{v}_i(t) \rangle \tag{4.4}$$

$$= \frac{1}{3N} \sum_{i=1}^{N} \lim_{t \to \infty} \frac{1}{2t} \langle [\delta \vec{r}_i(t)]^2 \rangle = D_{\rm s}(\theta = 0) = D_0, \tag{4.5}$$

which is precisely the self diffusivity at infinite dilution. This analysis confirms that the corrected diffusivity provides the proper generalization of self diffusion for collective transport phenomena, while the Fickian diffusivity combines both transport and thermodynamic properties.

While many interesting phenomenological simulations have been published on transport diffusion through nanopores, relatively few atomistic calculations have been carried out.[162] An important study was reported in 1993 by Maginn, Bell and Theodorou, developing non-equilibrium molecular dynamics calculations of methane transport diffusion through silicalite.[158] They applied gradient relaxation molecular dynamics (MD) as well as color field MD, simulating the equilibration of a macroscopic concentration gradient and the steady-state flow driven by an external field, respectively. They found indeed that the corrected diffusivity depends very weakly upon loading for this fluid-like system, and that the color field MD technique provides a more reliable method for simulating the linear response regime.

With the availability of high performance parallel supercomputers, there has been great interest in developing rigorous, grand canonical MD methods for modeling non-equilibrium transport through nanopores.[163–165] Despite the progress that has been made, these MD methods still suffer from the well known time scale problems discussed above for systems exhibiting rare event dynamics. As such, an important avenue for continued research is the development of realistic and illustrative lattice models for studying non-equilibrium diffusion in nanopores, especially because of recent progress in synthesizing continuous, oriented zeolite membranes.[166–169] These systems present new challenges to permeation theories because the finite extent of membranes in the transmembrane direction can produce interesting transport anomalies, as discussed below in Secs. IV A and Secs. IV B.

A. Anisotropy in Open Systems

Diffusion anisotropy in zeolites results from molecular jump rates that depend upon direction.[7,82] Diffusion anisotropy takes on special importance for permeation through oriented zeolite membranes, because the anisotropy introduced by a transmembrane concentration gradient can couple with the anisotropy inherent in a zeolite–guest system, yielding novel transport properties. For example, consider a 2-d square Langmuirian lattice

model. In this case, anisotropy leads to single-file transport through the membrane at one extreme, and single-file transport in the plane of the membrane in the other extreme. Although single-file motion at finite loadings exhibits normal concentration-independent, single-component transport diffusion, single-file motion gives rise to anomalous self diffusion, wherein the mean square displacement (MSD) is proportional at long times to $t^{1/2}$ rather than to t.[113,114,170−172] It is therefore of interest to investigate the signature of such anomalous self diffusion in a membrane transport system. However, since the long time limit of the MSD may not be accessible in a membrane of finite thickness, and since the natural observable in a permeation measurement is steady-state flux rather than the MSD, we need to imagine a convenient experiment that can probe this anomalous diffusion. Indeed, it has been shown that two-component, equimolar counter-permeation of identical, labeled species yields transport identical to self-diffusion.[155] Such a situation, hereafter denoted "tracer counter-permeation" (TCP),[29] is closely related to the tracer zero-length column experiment developed by Ruthven and co-workers.[126]

1. Tracer Counter-Permeation

The TCP simulation for a 2-d Langmuirian lattice model is shown in Fig. 15 below. We define the anisotropy parameter, η, according to $\eta = k_y/k_x$, where k_x and k_y are the elementary jump rates in the transmembrane and in-plane directions, respectively. $\eta = 1$ corresponds to an isotropic lattice, $\eta > 1$ corresponds to a membrane where the jump rate in the transmembrane direction is slower, and $\eta < 1$ corresponds a membrane where diffusion is faster in the transmembrane direction. The limiting case $\eta = 0$ corresponds to single-file diffusion. For example, the $\eta < 1$ case models p-xylene permeation through a silicalite membrane oriented along the b-axis, i.e. the straight channels, while $\eta > 1$ corresponds to the same system except oriented along the a-axis or c-axis,[166] i.e. the zig-zag or "corkscrew" channels, respectively. In Fig. 15, the parameters ν_A, ν_B and k_d control adsorption and desorption kinetics. We have parameterized this model based on data reported for cyclohexane in silicalite by Magalhães, Laurence and Conner,[173] as detailed in Ref. 29.
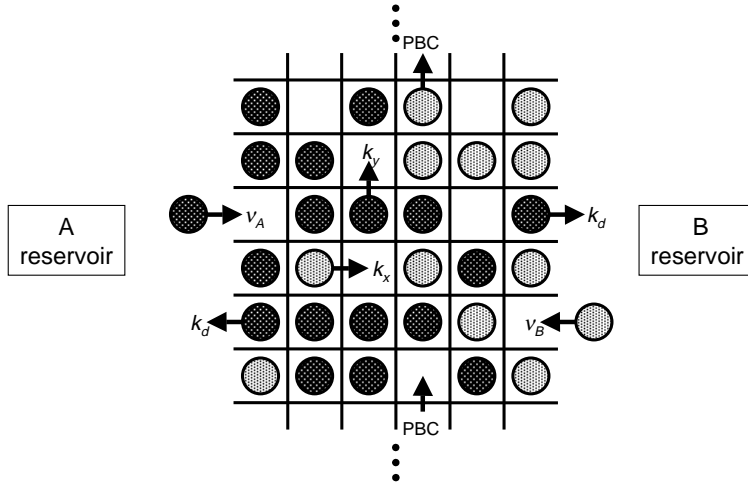
Figure 15. Schematic of a TCP simulation, with identical but differently labeled particles.

For such a system, it is well established that the scalar form of Fick's law should be replaced by a vector equation of the form:[29,30,153−156]

$$\begin{pmatrix} J_A \\ J_B \end{pmatrix} = - \begin{pmatrix} D_{AA} & D_{AB} \\ D_{BA} & D_{BB} \end{pmatrix} \begin{pmatrix} \nabla\theta_A \\ \nabla\theta_B \end{pmatrix}, \tag{4.6}$$

where θ_A and θ_B are the local loadings of components A and B, respectively. When species A and B have *identical* diffusive properties, the matrix in Eq. (4.6) is asymmetric, and has two eigenvectors that correspond to co-diffusion and counter-diffusion, the latter being relevant to TCP. The apparent diffusivities for counter-diffusion are given by :

$$D_A^+ = D_B^+ = D_0(1 - \theta_T)f(\theta_T) = D_s(\theta_T), \tag{4.7}$$

where $\theta_T = \theta_A + \theta_B$ is the total loading, which is constant throughout the lattice in TCP. $f(\theta_T)$ is the so-called correlation factor, a number between zero and one that measures the extent to which correlations diminish the self diffusivity from the MFT estimate (*cf.* the transmission coefficient and TST in Sec. II). Equation (4.7) shows that TCP can be used to model self diffusion in zeolites of finite extent.

We have developed and applied an open system KMC algorithm to explore the extent to which strong anisotropy can lead to anomalous self diffusion in zeolite membranes.[29] We have studied how the TCP-calculated self diffusivity depends upon membrane thickness L, and anisotropy η. When normal diffusion holds, the self diffusivity is independent of membrane thickness, i.e. is an intensive quantity, while anomalous diffusion is characterized by an L-dependent self diffusivity. Our simulations model cyclohexane in silicalite at $T = 656$ K with

a total fractional loading of $\theta_T = 0.9$. For convenience, we report the results in terms of the correlation factor, $f(L, \eta) = D_s/D_0(1 - \theta_T)$. For $\eta \gg 1$, we find that diffusion is normal and $f(L, \eta) \cong 1$, indicating that MFT becomes exact in this limit.[29] This is because sorbate motion in the plane of the membrane is very rapid, thereby washing out any correlations in the transmembrane direction. This is analogous to rapid $S_{II} \rightarrow S_{II}$ jumps washing out correlations in cage-to-cage motion of benzene in Na-Y,[31] which helps to explain why MFT works so well for that system.

As η is reduced, correlations between the motion of nearby molecules decrease the counter-diffusivity, as shown in Fig. 16 for $\eta = 0.01$, 0.001 and 0. The $\eta = 0.01$ diffusivities are independent of membrane thickness for all cases studied, and hence exhibit normal diffusion for membranes as thin as 10 sites across. On the other hand, the $\eta = 0.001$ diffusivities depend on membrane thickness for thin membranes, but approach a constant limiting value for thicker membranes. This indicates that for small values of η, a relatively large lattice is required to reach the thick membrane limit, such that particle exchange becomes probable during the intracrystalline lifetime. For thin membranes and small values of η, a diffusion mode with correlation lengths comparable to the membrane thickness, i.e. a global mode of diffusion, dominates. The extreme case of this occurs when $\eta = 0$ and diffusion is strictly single-file. In this type of lattice there is no localized mechanism for diffusion, and the diffusion coefficient always depends on system size, as shown in Fig. 16.
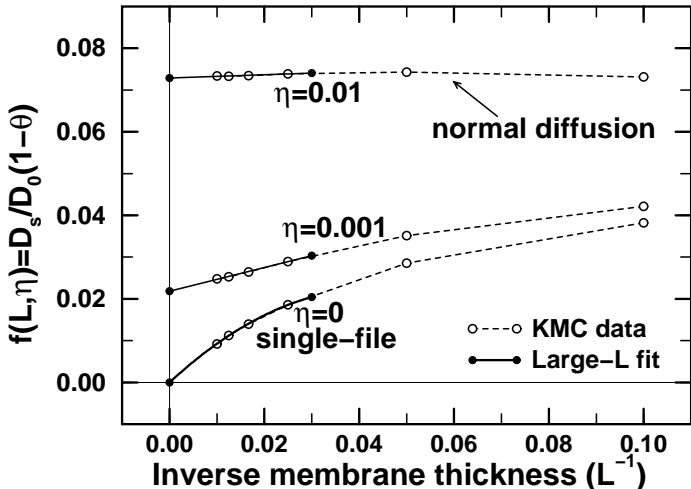

Figure 16. KMC calculated self diffusivities in membranes of various thicknesses and anisotropies, η, using the TCP method. $\eta > 0$ shows normal diffusion for sufficiently thick membranes, while $\eta = 0$ (single-file) is strictly anomalous.

The signature of anomalous self diffusion in single-file zeolite membranes is thus a diffusivity that decreases monotonically with membrane thickness. The findings in Fig. 16 suggest that the single-file self diffusivity scales as $\frac{1}{L}$, which can be understood with the following simple picture. In order for an A-particle to cross a single-file membrane, there must be no B-particles in the file. The probability that a given file contains no B particles scales as $\frac{1}{L}$. In Sec. IV B, we outline a theory for single-file self diffusion that accounts quantitatively for these anomalies using a vacancy-particle compound diffusion mechanism.[30]

B. Single-File Diffusion in Open Systems

In this section we explore a compound (two-stage) mechanism for diffusion in strictly single-file systems, wherein particle displacements of one lattice spacing are produced by a vacancy traversing the entire length of the file.[30] We begin by considering a single-file system of length $L = 6$ with TCP boundary conditions, as shown in Fig. 17. We imagine that the system is at steady-state with total occupancy close to one, so that on average there will be no more than a single vacancy in the file. Each of the states in Fig. 17(i)–(ix) is separated by an elementary jump event. The entire sequence in Fig. 17 entails a single vacancy entering on the A-side of the file, traveling through the file and subsequently leaving on the B-side. The net effect of the vacancy transport through the file is displacement of the particles by one lattice spacing to the left. Thus, a compound diffusion mechanism operates in single-file systems, which requires a vacancy to diffuse the entire file length to generate particle displacements of one lattice spacing.
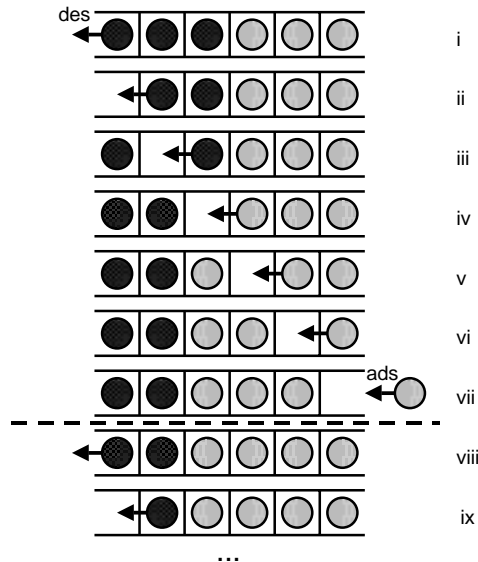
Figure 17. Vacancy transport through an $L = 6$ single-file system, with A-particles (dark) and B-particles (light). Steps (i) through (vii) represent the passage of an "A-vacancy" from right to left, giving particle displacement of one lattice spacing in the opposite direction.

We now consider a thought experiment where vacancies within the lattice are labeled by the side of the lattice on which they were created, e.g. an A-vacancy is created in the transition from steps (i) to (ii) in Fig. 17. In fact, an A-vacancy is created whenever a particle of either type desorbs into the A-phase. In Fig. 17(vii), the A-vacancy exchanges with a B-particle from the external B-phase. With this interpretation, we have a steady-state flux of A-vacancies from left to right through the lattice, and *vice versa* for the B-vacancies, while unlabeled vacancies have no net flux.

We now derive the L-dependence of D_s assuming that the flux of A-vacancies obeys Fick's law:

$$J_A^V = -D_A^V \nabla \theta_A^V, \tag{4.8}$$

where $\nabla \theta_A^V$ is the A-vacancy concentration gradient, and D_A^V is the apparent diffusivity of A-vacancies. At infinite vacancy dilution, D_A^V is equal to D_0, the single-component particle transport diffusivity. Inspired by the compound diffusion picture developed above, we further assume that the flux of B-particles is related to the flux of A-vacancies by the following *ansatz*:

$$J_B = -\frac{J_A^V}{L-1}. \tag{4.9}$$

The factor of $(L-1)^{-1}$ arises because an A-vacancy must traverse the length of the file, as shown in Fig. 17, to move particles by one lattice spacing. By exploiting the properties of steady-state TCP, these assumptions lead to the following expression for D_s:

$$D_s = \frac{D_0 \theta_T k_d^2 (L-1)}{(1-\theta_T)(L-1)\nu[\nu(L-1) + 2D_0] - 2D_0 \theta_T k_d}. \tag{4.10}$$

Equation (4.10) agrees quantitatively with results from open system KMC simulations under TCP boundary conditions.[30] Furthermore, in the limit that $L \to \infty$, the expression in Eq. (4.10) becomes:

$$D_s = \frac{D_0 (1 - \theta_T)}{L \theta_T}, \tag{4.11}$$

which is precisely the expression recently obtained by Hahn and Kärger for the self diffusion coefficient associated with center-of-mass motion of particles within the file.[174] Hahn and Kärger obtained their expression by analyzing the Gaussian statistics of several correlated random walkers in a single-file system. Our derivation of Eq. (4.11) shows that Hahn and Kärger's result is consistent with assuming that transport is diffusion-limited, which becomes valid in the long-file limit. Our result in Eq. (4.10) is also valid for short files, which exhibit sorption-limited transport.

We find it intriguing that a self-diffusion coefficient can be meaningfully defined and derived for a strictly single-file system, albeit of finite extent. It is irresistible to wonder whether mean square displacements (MSDs) for this system can exhibit the $t^{1/2}$ behavior that characterizes single-file systems of *infinite* extent. To address this question, we calculated MSDs using open system KMC as follows. An $L = 60$ single-file system was initially filled with particles up to an average occupancy of $\theta_T = 0.9$ throughout. Particles in column 30 were labeled as B-particles, while the remainder were labeled as A-particles. At $t = 0$, both edges of the system were exposed to a phase of A-particles with an insertion rate that maintained the equilibrium A-occupancy at $\theta_A = 0.9$.

The results are shown in Fig. 18 on a log-log plot. The dotted lines have slope equal to 1 indicating that the MSD is proportional to t, whereas the dashed line has a slope of $\frac{1}{2}$ indicating that the MSD is proportional to $t^{1/2}$. The short time behavior is consistent with

mean field theory, where the dotted line is given by Einstein's equation with $D_s = D_0(1-\theta_T)$. At long times, the MSD in Fig. 18 (middle dotted line) is again given by Einstein's equation with D_s given by Eq. (4.10), giving transport that is dominated by compound diffusion. At intermediate times, transport is achieved by a single-file mode that operates as if the file were of infinite extent, with an MSD given by $\langle R^2(t) \rangle = 2Ft^{1/2}$, where F is the single-file mobility.[153,174]
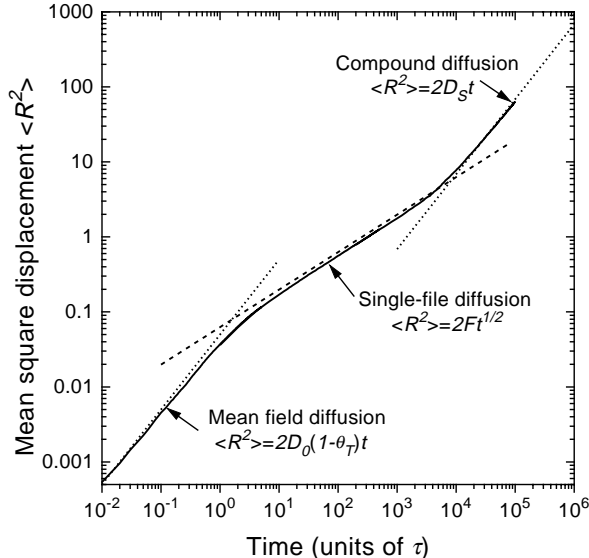

Figure 18. Log-log plot of MSDs calculated with KMC and theory for an $L = 60$ single-file system; from simulation (solid line), MFT (left-most dotted line), single-file diffusion theory with slope of $\frac{1}{2}$ (dashed line), and compound diffusion theory giving slope of 1 (middle and right-most dotted lines).

Using the theory derived above, the crossover time between single-file diffusion and compound diffusion in long files is given by $t_c = L^2/\pi D_0$, which is precisely the formula obtained by Hahn and Kärger,[174] and is proportional to the characteristic time for vacancy diffusion through the system.[175] That is, by the time a vacancy has traversed the file, the extent of correlations becomes comparable to the file length, the compound diffusion mechanism dominates, and the MSD is once again governed by Einstein's equation, with a diffusivity that is greatly diminished by correlations according to Eq. (4.10). Hence, the file edges influence the motion of all particles *long before* they reach the file edges.

Typical parameters for zeolite membrane permeation are $L = 10$ μm and $D_0 = 10^{-6}$ cm^{2}s^{-1}. These parameters give a crossover time of $t_c \cong 0.3$ s, which happens to fall just above the experimental window of observation for PFG NMR.[170] We therefore predict that PFG NMR measurements extended to longer times will observe that MSDs crossover from $t^{1/2}$ to normal Fickian behavior, except with a long-time single-file self diffusivity that depends upon system size.

Although the duration of single-file diffusion increases with file length, the relative importance of single-file motion decreases with file length. This becomes clear by analyzing

the fraction of time that particles spend single-file diffusing while adsorbed in a zeolite crystallite. This fraction is given by t_c/τ_{intra}, where t_c is the crossover time and τ_{intra} is the intra-crystalline residence time,[172] which scales as L^2/D_s. Since $t_c \propto L^2$ while $D_s \propto 1/L$ for long files, we see that the fraction of time in single-file diffusion mode scales as $1/L$ for long files. Ironically, while single-file diffusion is more easily measured in longer files, compound diffusion becomes the dominant transport process in larger zeolite particles.

V. CONCLUDING REMARKS

In this review, we have explored the interplay among dynamics, diffusion and phase equilibrium in nanopores. We have focused on atomistic and lattice models of small to medium guest molecules in zeolite molecular sieves, because of their great importance and versatility in science and industry. As a common theme running through the review, we have highlighted our own calculations on benzene in Na-X and Na-Y zeolites, because of persistent, qualitative discrepancies between different experimental probes of self diffusion for these systems.

We began by discussing the theory and practice of modeling rare event dynamics in zeolites, by considering how researchers develop forcefields and implement transition state theory (TST) with dynamical corrections. We find that site-to-site jump dynamics in zeolites are well described by TST when the initial or final sites involve relatively deep potential mimina, and that molecular jump dynamics in a large pore zeolite is well described by including only a small number of degrees of freedom. Challenges for future modeling include direct *ab initio* parameterization of TST calculations on zeolites, TST with flexible lattices for tight-fitting zeolite–guest systems, and TST applied to molecules in zeolites at finite loadings. Solving the latter two problems will require progress in defining high dimensional dividing surfaces.

Based on kinetic Monte Carlo (KMC) simulations of benzene in Na-Y, we have shown that non-exponential decay of the orientational correlation function can disentangle the rates of intracage and intercage motion, and may indicate heterogeneous aluminum agglomeration, leading to new NMR probes of zeolite structure. In general, we believe that such modeling should be regarded as a characterization tool complementary to diffraction, NMR, IR, etc. The impact of such modeling will grow by maintaining close connections with practitioners of experimental characterization.

We then considered many-body adsorption and diffusion in zeolites, in an effort to begin bridging the gap between these two fields. We focused on mean field theory (MFT) and KMC applied to lattice models, which are natural for systems dominated by jump diffusion. Modeling many-body diffusion in zeolites remains challenging because of the coupling between rare event dynamics and strong guest–guest interactions. To address this, we outlined a model for determining how guest–guest interactions modify activation energies of site-to-site jumps. Based on this model, our calculations for benzene in Na-X give excellent qualitative agreement with PFG NMR diffusivities, and give qualitative disagreement with TZLC data. We then explored the possibility that benzene can undergo phase transitions from low to high sorbate density in Na-X, analogous to vapor–liquid equilibrium of bulk benzene. Although our calculations suggest a critical temperature of 370 K, this result is

exquisitely sensitive to errors in the model. By exploring the impact of this type of phase transition on diffusion in zeolites, we explain intriguing loading dependencies of water and ammonia diffusion in terms of a subcritical droplet picture of adsorption in zeolites. In general, we find that understanding the thermodynamics of confined fluids can be crucial for elucidating the transport properties of molecules in zeolites.

Finally, we discussed various formulations of non-equilibrium diffusion through lattice models of finite extent. We suggested that computing cross-correlated mean square displacements may provide a feasible equilibrium approach for modeling non-equilibrium diffusion in zeolites. We described a tracer counter-permeation KMC algorithm, to search for the steady-state signature of anomalous transport in finite single-file systems. Our theory and simulations show that transport in finite single-file systems is characterized by a diffusivity that decreases monotonically with file length. Hence, except for the fact that this diffusivity depends on file length, self diffusion in single-file systems is Fickian in the sense that Fick's first and second laws are obeyed for a file of given length. We discussed the experimental implications of this finding in the context of PFG NMR observation times. In general, we have found that explicitly including adsorption and desorption phenomena in open system diffusion models is crucial for drawing qualitatively valid conclusions regarding single-file diffusion.

We hope that these computational studies can assist in the design of new materials with advanced performance by elucidating the microscopic factors that control adsorption, diffusion and reaction in zeolites. While this dream is not yet an everyday reality, examples exist today that have the flavor of rational design.[176] We believe that such design will become much more commonplace within the next ten years, with the advent of better algorithms and faster computers. Perhaps even more significant is the prospect for cross-fertilization between zeolite science and other fields. For example, it is intriguing to wonder whether single-file diffusion through biological ion channels in cell membranes[177] occurs *via* the compound diffusion mechanism described above. Answering such a question will require even *further* breakthroughs in our understanding of dynamics and diffusion in nanopores.

REFERENCES

[1] D. W. Breck. *Zeolite Molecular Sieves: Structure, Chemistry and Use*. Wiley, New York, 1974.

[2] R. M. Barrer. *Zeolites and Clay Minerals as Sorbents and Molecular Sieves*. Academic Press, London, 1978.

[3] H. van Bekkum, E. M. Flanigen, and J. C. Jansen, editors. *Introduction to Zeolite Science and Practice*. Elsevier, Amsterdam, 1991.

[4] D. H. Olson, W. M. Meier, and C. Baerlocher. *Atlas of Zeolite Structure Types*. Elsevier, London, 1996.

[5] International Zeolite Association. Atlas of zeolite structure types. <http://www.iza-sc.ethz.ch/IZA-SC/Atlas/AtlasHome.html>.

[6] J. Weitkamp. In G. Olhmann, J. C. Vedrine, and P. A. Jacobs, editors, *Catalysis and Adsorption by Zeolites*, page 21. Elsevier, Amsterdam, 1991.

[7] J. Kärger and D. M. Ruthven. *Diffusion in Zeolites and Other Microporous Solids*. John Wiley & Sons, New York, 1992.

[8] N. Y. Chen, T. F. Degnan, Jr., and C. M. Smith. *Molecular Transport and Reaction in Zeolites*. VCH Publishers, New York, 1994.

[9] J. M. Newsam. Zeolites. In A. K. Cheetham and P. Day, editors, *Solid State Chemistry: Compounds*, pages 234–280. Oxford University Press, Oxford, 1992.

[10] S. M. Kuznicki, K. A. Thrush, and H. M. Garfinkel, 1993. US Patent (pending).

[11] *Chem. and Eng. News*, 74(11):29, 1996.

[12] C. T. Kresge, M. E. Leonowicz, W. J. Roth, J. C. Vartuli, and J. S. Beck. *Nature*, 359:710, 1992.

[13] C. R. A. Catlow, editor. *Modelling of Structure and Reactivity in Zeolites*. Academic Press, London, 1992.

[14] P. Demontis and G. B. Suffritti. *Chem. Rev.*, 97:2845, 1997. and references therein.

[15] M. W. Deem. *AICHE J.*, 44:2569, 1998.

[16] S. M. Auerbach, N. J. Henson, A. K. Cheetham, and H. I. Metiu. *J. Phys. Chem.*, 99:10600, 1995.

[17] S. M. Auerbach, L. M. Bull, N. J. Henson, H. I. Metiu, and A. K. Cheetham. *J. Phys. Chem.*, 100:5923, 1996.

[18] S. M. Auerbach and H. I. Metiu. *J. Chem. Phys.*, 105:3753, 1996.

[19] S. M. Auerbach and H. I. Metiu. *J. Chem. Phys.*, 106:2893, 1997.

[20] S. M. Auerbach. *J. Chem. Phys.*, 106:7810, 1997.

[21] C. Saravanan and S. M. Auerbach. *J. Chem. Phys.*, 107:8120, 1997.

[22] C. Saravanan and S. M. Auerbach. *J. Chem. Phys.*, 107:8132, 1997.

[23] F. Jousse and S. M. Auerbach. *J. Chem. Phys.*, 107:9629, 1997.

[24] C. Saravanan, F. Jousse, and S. M. Auerbach. *J. Chem. Phys.*, 108:2162, 1998.

[25] C. Saravanan, F. Jousse, and S. M. Auerbach. *Phys. Rev. Lett.*, 80:5754, 1998.

[26] F. Jousse, S. M. Auerbach, and D. P. Vercauteren. *J. Phys. Chem. B*, 102:6507, 1998.

[27] D. E. Favre, D. J. Schaefer, S. M. Auerbach, and B. F. Chmelka. *Phys. Rev. Lett.*, 81:5852, 1998.

[28] C. Saravanan and S. M. Auerbach. *J. Chem. Phys.*, 109:8755, 1998.

[29] P. H. Nelson and S. M. Auerbach. *invited by Chem. Eng. J.*, 74:43, 1999.

[30] P. H. Nelson and S. M. Auerbach. *J. Chem. Phys.*, 110:9235, 1999.

[31] C. Saravanan and S. M. Auerbach. *J. Chem. Phys.*, 110:11000, 1999.

[32] E. Jaramillo and S. M. Auerbach. *J. Phys. Chem. B*, 1999. in press.

[33] F. Jousse, S. M. Auerbach, and D. P. Vercauteren. *J. Chem. Phys.*, 1999. submitted.

[34] J. T. Fermann, C. Blanco, and S. M. Auerbach. *J. Chem. Phys.*, 1999. submitted.

[35] J. T. Fermann and S. M. Auerbach. *J. Chem. Phys.*, 1999. submitted.

[36] R. Gomer. *Rep. Prog. Phys.*, 53:917, 1990.

[37] D. A. Dougherty. *Science*, 271:163, 1996.

[38] C. Tunca and D. M. Ford. *J. Chem. Phys.*, 111:2751, 1999.

[39] D. Chandler. *Introduction to Modern Statistical Mechanics*. Oxford University Press, New York, 1987.

[40] R. Car and M. Parrinello. *Phys. Rev. Lett.*, 55:2471, 1995.

[41] L. Campana, A. Selloni, J. Weber, A. Pasquarello, I. Papai, and A. Goursot. *Chem. Phys. Lett.*, 226:245–250, 1994.

[42] L. Campana, A. Selloni, J. Weber, and A. Goursot. *J. Phys. Chem.*, 99(44):16351–16356, 1995.

[43] V. Termath, F. Haase, J. Sauer, J. Hutter, and M. Parrinello. *J. Am. Chem. Soc.*, 120:8512, 1998.

[44] C. M. Freeman, D. W. Lewis, T. V. Harris, A. K. Cheetham, N. J. Henson, P. A. Cox, A. M. Gorman, S. M. Levine, J. M. Newsam, E. Hernandez, and C. R. A. Catlow. *ACS Sym. Ser.*, 589:326, 1995. and references therein.

[45] C. R. A. Catlow, C. M. Freeman, B. Vessal, S. M. Tomlinson, and M. Leslie. *J. Chem. Soc., Faraday Trans.*, 87:1947, 1991.

[46] M. F. Allen and D. J. Tildesley. *Computer Simulation of Liquids*. Oxford Science Publications, Oxford, 1987.

[47] L. Greengard and V. Rokhlin. *J. Comp. Phys.*, 73:325–348, 1987.

[48] J. Sauer. *Chem. Rev.*, 98:199, 1989. and references therein.

[49] R. A. van Santen and G. J. Kramer. *Chem. Rev.*, 95:637, 1995. and references therein.

[50] M. Cook and W. C. Conner. How big are the pores of zeolites? In M. M. J. Treacy, B. K. Marcus, M. E. Bisher, and J. B. Higgins, editors, *Proceedings of the 12*th *International Zeolite Conference*, pages 409–414. Materials Research Society, Warrendale, PA, 1999.

[51] B. K. Peterson. *J. Phys. Chem. B*, 103:3145, 1999.

[52] G. Vitale, C. F. Mellot, L. M. Bull, and A. K. Cheetham. *J. Phys. Chem. B*, 101:4559, 1997.

[53] D. G. Truhlar and B. C. Garrett. *Ann. Rev. Phys. Chem.*, 35:159, 1984.

[54] S. C. Tucker and D. G. Truhlar. Dynamical formulation of transition state theory. In J. Bertran and I. G. Csizmadia, editors, *New Theoretical Concepts for Understanding Organic Reactions*, page 291. Kluwer, Dordrecht, The Netherlands, 1989.

[55] T. N. Truong. *J. Phys. Chem. B*, 101:2750, 1997.

[56] R. Shah, M. C. Payne, M.-H. Lee, and J. D. Gale. *Science*, 271:1395, 1996.

[57] J. P. Carter, R. P. Grosso, and S. M. Auerbach. manuscript in preparation, 1999.

[58] N. J. Henson, A. K. Cheetham, M. Stockenhuber, and J. A. Lercher. *J. Chem. Soc., Faraday Trans.*, 94:3759, 1998.

[59] L. M. Bull, N. J. Henson, A. K. Cheetham, J. M. Newsam, and S. J. Heyes. *J. Phys. Chem.*, 97:11776, 1993.

[60] N. J. Henson, S. M. Auerbach, and B. K. Peterson, 1999. Dizzy: Dynamics in Zeolites.

[61] L. Uytterhoeven, D. Dompas, and W. J. Mortier. *J. Chem. Soc., Faraday Trans.*, 88:2753,

1992.

[62] H. Klein, C. Kirschhock, and H. Fuess. *J. Phys. Chem.*, 98:12345, 1994.

[63] T. Mosell, G. Schrimpf, and J. Brickmann. *J. Phys. Chem. B*, 101:9476, 1997.

[64] A. N. Fitch, H. Jobic, and A. Renouprez. *J. Phys. Chem.*, 90:1311, 1986.

[65] O. Isfort, B. Boddenberg, F. Fujara, and R. Grosse. *Chem. Phys. Lett.*, 288:71, 1998.

[66] H. Jobic, private communication.

[67] H. Blank, M. Bülow, and W. Schirmer. *Z. Phys. Chemie.*, 260:395, 1979.

[68] D. J. Schaefer, D. E. Favre, M. Wilhelm, S. J. Weigel, and B. F. Chmelka. *J. Am. Chem. Soc.*, 119:9252, 1997.

[69] D. Barthomeuf and B. H. Ha. *J. Chem. Soc., Faraday Trans.*, 69:2158, 1973.

[70] W. H. Miller. *J. Chem. Phys.*, 61:1823, 1974.

[71] D. Chandler. *J. Chem. Phys.*, 68:2959, 1978.

[72] A. F. Voter and J. D. Doll. *J. Chem. Phys.*, 82:80, 1985.

[73] G. A. Voth, D. Chandler, and W. H. Miller. *J. Chem. Phys.*, 91:7749, 1989.

[74] G. H. Vineyard. *J. Phys. Chem. Solids*, 3:121, 1957.

[75] E. M. Sevick, A. T. Bell, and D. N. Theodorou. *J. Chem. Phys.*, 98:3196, 1993.

[76] H. Jonsson, G. Mills, and K. W. Jacobsen. Nudged elastic band method for finding minimum energy paths of transitions. In B. J. Berne, G. Ciccotti, and D. F. Coker, editors, *Classical and Quantum Dynamics in Condensed Phase Simulations*, page 385. World Scientific, 1998.

[77] A. Voter. *J. Chem. Phys.*, 106:4665, 1997.

[78] C. Dellago, P. G. Bolhuis, F. S. Csajka, and D. Chandler. *J. Chem. Phys.*, 108:1964, 1998.

[79] P. Demontis, S. Yashonath, and M. L. Klein. *J. Phys. Chem.*, 93:5016, 1989.

[80] R. L. June, A. T. Bell, and D. N. Theodorou. *J. Phys. Chem.*, 95:8866, 1991.

[81] J. Kärger, P. Demontis, G. B. Suffritti, and A. Tilocca. *J. Chem. Phys.*, 110:1163, 1999.

[82] J. Kärger. *J. Phys. Chem.*, 95:5558, 1991.

[83] R. Q. Snurr, A. T. Bell, and D. N. Theodorou. *J. Phys. Chem.*, 98:11948, 1994.

[84] E. J. Maginn, A. T. Bell, and D. N. Theodorou. *J. Phys. Chem.*, 100:7155, 1996.

[85] M. L. Greenfield and D. N. Theodorou. *Macromolecules*, 31:7068, 1998.

[86] F. Jousse, L. Leherte, and D. P. Vercauteren. *J. Phys. Chem. B*, 101:4717, 1997.

[87] T. Mosell, G. Schrimpf, C. Hahn, and J. Brickmann. *J. Phys. Chem.*, 100:4571, 1996.

[88] T. Mosell, G. Schrimpf, and J. Brickmann. *J. Phys. Chem.*, 100:4582, 1996.

[89] T. Mosell, G. Schrimpf, and J. Brickmann. *J. Phys. Chem. B*, 101:9485, 1997.

[90] A. Voter. *J. Chem. Phys.*, 82:1890, 1985.

[91] C. Saravanan, F. Jousse, and S. M. Auerbach. *ACS Sym. Ser.*, 721:296, 1999.

[92] K. A. Fichthorn and W. H. Weinberg. *J. Chem. Phys.*, 95:1090, 1991.

[93] H. I. Metiu, Y. T. Lu, and Z. Y. Zhang. *Science*, 255:1088, 1992.

[94] C. Saravanan. PhD thesis, University of Massachusetts at Amherst, 1999.

[95] P. Maksym. *Semicond. Sci. Technol.*, 3:594, 1988.

[96] P. H. Nelson, A. B. Kaiser, and D. M. Bibby. *J. Catal.*, 127:101, 1991.

[97] M. Bülow, U. Härtel, U. Müller, and K. K. Unger. *Ber. Bunsen-Ges. Phys. Chem.*, 94:74, 1990.

[98] D. Shen and L. V. C. Rees. *J. Chem. Soc., Faraday Trans.*, 86:3687, 1990.

[99] P. R. van Tassel, S. A. Somers, H. T. Davis, and A. V. McCormick. *Chem. Eng. Sci.*,

49:2979, 1994.

[100] W. Heink, J. Kärger, H. Pfeifer, and F. Stallmach. *J. Am. Chem. Soc.*, 112:2175, 1990.

[101] S. Yashonath. *J. Phys. Chem.*, 95:5877, 1991.

[102] C. J. Jameson, A. K. Jameson, R. Gerald, and A. C. de Dios. *J. Chem. Phys.*, 96:1676, 1992.

[103] R. C. Tolman. *The Principles of Statistical Mechanics*. Oxford University Press, New York, 1938.

[104] L. A. Clark, G. T. Ye, A. Gupta, L. L. Hall, and R. Q. Snurr. *J. Chem. Phys.*, 111:1209, 1999.

[105] O. M. Braun and C. A. Sholl. *Phys. Rev. B*, 58:14870, 1998.

[106] K. Schmidt-Rohr and H. W. Spiess. *Multidimensional Solid-State NMR and Polymers*. Academic Press, London, 1994.

[107] H. Klein, H. Fuess, and G. Schrimpf. *J. Phys. Chem.*, 100:11101, 1996.

[108] B. Boddenberg and R. Burmeister. *Zeolites*, 8:488, 1988.

[109] B. Boddenberg and B. Beerwerth. *J. Phys. Chem.*, 93:1440, 1989.

[110] R. Burmeister, H. Schwarz, and B. Boddenberg. *Ber. Bunsenges. Phys. Chem.*, 93:1309, 1989.

[111] A. Germanus, J. Kärger, H. Pfeifer, N. N. Samulevic, and S. P. Zdanov. *Zeolites*, 5:91, 1985.

[112] M. T. Melchior, D. E. W. Vaughan, and C. F. Pictroski. *J. Phys. Chem.*, 99:6128, 1995.

[113] K. Hahn, J. Kärger, and V. Kukla. *Phys. Rev. Lett.*, 76(15):2762, 1996.

[114] V. Gupta, S. S. Nivarthi, D. Keffer, A. V. McCormick, and H. T. Davis. *Science*, 274:164, 1996.

[115] D. S. Sholl and K. A. Fichthorn. *Phys. Rev. Lett.*, 79:3569, 1997.

[116] D. Keffer, A. V. McCormick, and H. T. Davis. *J. Phys. Chem.*, 100:967, 1996.

[117] R. Q. Snurr. Special issue devoted to molecular modeling of transport; see references therein. *Chem. Eng. J.*, 74, 1999.

[118] D. N. Theodorou and J. Wei. *J. Catal.*, 83:205, 1990.

[119] P. H. Nelson, A. B. Kaiser, and D. M. Bibby. *Zeolites*, 11:337, 1991.

[120] P. H. Nelson and D. M. Bibby. *Stud. Surf. Sci. Catal.*, 68:407, 1991.

[121] D. Stauffer and A. Aharony. *Introduction to Percolation Theory*. Taylor & Francis, Inc., Bristol, PA, 1991.

[122] M. O. Coppens, A. T. Bell, and A. K. Chakraborty. *Chem. Eng. Sci.*, 53:2053, 1998.

[123] J. Kärger and H. Pfeifer. *Zeolites*, 7:90, 1987.

[124] B. L. Trout, A. K. Chakraborty, and A. T. Bell. *J. Phys. Chem.*, 100:17582, 1996.

[125] B. L. Trout, A. K. Chakraborty, and A. T. Bell. *Chem. Eng. Sci.*, 52:2265, 1997.

[126] S. Brandani, Z. Xu, and D. Ruthven. *Microporous Materials*, 7:323, 1996.

[127] M. O. Coppens, A. T. Bell, and A. K. Chakraborty. *Chem. Eng. Sci.*, 54:3455, 1999.

[128] C. Rodenbeck, J. Kärger, and K. Hahn. *Phys. Rev. E*, 55:5697, 1997.

[129] R. Krishna, B. Smit, and T. J. H. Vlugt. *J. Phys. Chem.* **A**, 102:7727, 1998.

[130] R. Krishna, T. J. H. Vlugt, and B. Smit. *Chem. Eng. Sci.*, 54:1751, 1999.

[131] D. H. Olson. *Zeolites*, 15:439, 1995.

[132] D. Barthomeuf and B. H. Ha. *J. Chem. Soc., Faraday Trans.*, 69:2147, 1973.

[133] E. S. Hood, B. H. Toby, and W. H. Weinberg. *Phys. Rev. Lett.*, 55:2437, 1985.

[134] T. Hjelt, I. Vattulainen, J. Merikoski, and T. Ala-Nissila *et al. Surf. Sci.*, 380:501, 1997.

[135] M. Bülow, W. Mietk, P. Struve, and P. Lorenz. *J. Chem. Soc., Faraday Trans. I*, 79:2457, 1983.

[136] H. Jobic, M. Bée, J. Kärger, H. Pfeifer, and J. Caro. *J. Chem. Soc., Chem. Commun.*, (4):341, 1990.

[137] D. M. Shen and L. V. C. Rees. *Zeolites*, 11:666, 1991.

[138] S. J. Gregg and K. S. W. Sing. *Adsorption, Surface Area and Porosity*. Academic Press, New York, 1982.

[139] J. Fraissard and W. C. Conner, Jr., editors. *Physical Adsorption: Experiment, Theory and Applications*. Kluwer Academic Publishers, Boston, 1997.

[140] C. Martin, J.-P. Coulomb, Y. Grillet, and R. Kahn. In M. D. LeVan, editor, *Fundamentals of Adsorption: Proceedings of the Fifth International Conference*. Kluwer Academic Publishers, Boston, 1996.

[141] R. Radhakrishnan and K. E. Gubbins. *Phys. Rev. Lett.*, 79:2847, 1997.

[142] T. Maris, T. J. H. Vlugt, and B. Smit. *J. Phys. Chem.* **B**, 102:7183, 1998.

[143] J. G. Pearson, B. F. Chmelka, D. N. Shykind, and A. Pines. *J. Phys. Chem.*, 96:8517, 1992.

[144] B. K. Peterson and K. E. Gubbins. *Mol. Phys.*, 62:215, 1987.

[145] K. S. Page and P.A. Monson. *Phys. Rev. E*, 54:6557, 1996.

[146] R. H. Swendsen and J.-S. Wang. *Phys. Rev. Lett.*, 58:86, 1987.

[147] U. Wolff. *Phys. Rev. Lett.*, 62:361, 1989.

[148] O. Redner, J. Machta, and L. F. Chayes. *Phys. Rev. E*, 58:2749, 1997.

[149] P. M. Chaikin and T. C. Lubensky. *Principles of Condensed Matter Physics*. Cambridge University Press, New York, 1992.

[150] O. H. Tezel and D. M. Ruthven. *J. Coll. Inter. Sci.*, 139:581, 1990.

[151] D. Frenkel and B. Smit. *Understanding Molecular Simulations*. Academic Press, San Diego, 1996.

[152] V. Lachet, A. Boutin, B. Tavitian, and A. H. Fuchs. *J. Phys. Chem. B*, 102:9224, 1998.

[153] K. W. Kehr, K. Binder, and S. M. Reulein. *Phys. Rev. B*, 39:4891, 1989.

[154] W. R. Qureshi and J. Wei. *J. Catal.*, 126:126, 1990.

[155] P. H. Nelson and J. Wei. *J. Catal.*, 136:263, 1992.

[156] K. Binder. *Rep. Prog. Phys.*, 60:487, 1997.

[157] R. Kutner. *Phys. Lett. A*, 81:239, 1981.

[158] E. J. Maginn, A. T. Bell, and D. N. Theodorou. *J. Phys. Chem.*, 97:4173, 1993.

[159] R. Krishna. *Chem. Eng. Sci.*, 48:845, 1993.

[160] M. Gaub, S. Fritzsche, R. Haberlandt, and D. N. Theodorou. *J. Phys. Chem. B*, 103:4721, 1999.

[161] I. V. Belova and G. E. Murch. *Philos. Mag. A*, 78:1085, 1998.

[162] C. J. Mundy, S. Balasubramanian, K. Bagchi, M. E. Tuckerman, G. J. Martyna, and M. L. Klein. *Rev. of Comp. Chem.*, 1999. in press.

[163] R. F. Cracknell, D. Nicholson, and N. Quirke. *Phys. Rev. Lett.*, 74:2463, 1995.

[164] P. I. Pohl, G. S. Heffelfinger, and D. M. Smith. *Mol. Phys.*, 89:1725, 1996.

[165] A. P. Thompson, D. M. Ford, and G. S. Heffelfinger. *J. Chem. Phys.*, 109:6406, 1999.

[166] M. C. Lovallo and M. Tsapatsis. *AIChE Journal*, 42:3020, 1996.

[167] W. J. W. Bakker, F. Kapteijn, J. Poppe, and J. A. Moulijn. *J. Membrane Sci.*, 117:57, 1996.

[168] C. D. Baertsch, H. H. Funke, J. L. Falconer, and R. D. Noble. *J. Phys. Chem.*, 100:7676, 1996.

[169] A. J. Burggraaf, Z. A. E. P. Vroon, K. Keizer, and H. Verweij. *J. Membrane Sci.*, 144:77, 1998.

[170] J. Kärger, G. Fleischer, and U. Roland. PFG NMR studies of anomalous diffusion. In J. Kärger, Paul Heitjans, and Reinhold Haberlandt, editors, *Diffusion in Condensed Matter*, pages 143–168. Hubert & Co., Göttingen, 1998. and references therein.

[171] R. Haberlandt and J. Kärger. *Chem. Eng. J.*, 74:15, 1999.

[172] J. Kärger. Single-file diffusion in zeolites. In H. G. Karge and J. Weitkamp, editors, *Molecular Sieves - Science and Technology Vol. 7: Sorption and Diffusion*. Springer-Verlag, Berlin, New York, 1999. and references therein.

[173] F. D. Magalhães, R. L. Laurence, and W. C. Conner. *J. Phys. Chem. B*, 102:2317, 1998.

[174] K. Hahn and J. Kärger. *J. Phys. Chem. B*, 102:5766, 1998.

[175] J. Crank. *The Mathematics of Diffusion, 2nd edition*. Oxford University Press, 1978.

[176] C. C. Freyhardt, M. Tsapatsis, R. F. Lobo, K. J. Balkus, M. E. Davis, et al. *Nature*, 381:295, 1996.

[177] R. S. Eisenberg. *Acc. Chem. Res.*, 31:117, 1998.

TABLE I. Experiment and theory for benzene energetics (kJ mol^{-1}) in various FAU-type zeolites.

Zeolite	Exp $|\Delta H_{\mathrm{sorb}}|$	ref	Theo $|\Delta H_{\mathrm{sorb}}|$	ref	Exp E_a	ref	Theo E_a	ref
Ca-X	134	67	119	27	62	68	75	27
Na-X	73	69	70	17	14	17	15	17
Na-Y	79	69	77	16	24	59	35	16
Si-Y	55	58	59	57	10	59	7	57

TABLE II. Apparent Arrhenius parameters from rate coefficients for benzene jumps among S_{II} and W sites in Na-Y, using TST and RFCT methods. Note the failure of TST for the W→W jump.

	Activation Energy (kJ mol^{-1})			Arrhenius Prefactors	
Jump Process	MEP	TST	RFCT	TST	RFCT
W→S$_{II}$	16	17.0 ± 0.1	16.4 ± 0.3	2.7 10^{12} s^{-1}	1.1 10^{12} s^{-1}
W→W	18	→ 1.1± 0.5 ←	15.1 ± 4.0	6.0 10^{11} s^{-1}	2.4 10^{11} s^{-1}
S$_{II}$→W	41	44.8 ± 0.1	44.4 ± 0.1	1.6 10^{13} s^{-1}	0.8 10^{13} s^{-1}
S$_{II}$→S$_{II}$	35	37.4 ± 0.1	36.8 ± 0.3	1.6 10^{13} s^{-1}	0.8 10^{13} s^{-1}
K_{eq}(S$_{II}$→W)	25	28.0 ± 0.2		7.1	

TABLE III. Best available activation energies (kJ mol^{-1}) for benzene jumps at infinite dilution in Na-X and Na-Y.

	Na-Y	Na-X
S$_{II}$→S$_{II}$	25	15
S$_{II}$→W	38	25
W→S$_{II}$	13	10
W→W	13	10

FIGURES

FIG. 1. Development of schematic lattice for zeolite–guest systems.

FIG. 2. Specific lattice geometry for benzene in Na-Y zeolite.

FIG. 3. Sorption sites and jumps for benzene in Na-Y.

FIG. 4. $S_{II} \leftrightarrow W$ MEP for benzene in Na-Y (transition state indicated in bold), with a calculated barrier of 41 kJ mol^{-1}.

FIG. 5. Schematic of dividing surfaces for benzene jumps in Na-Y.

FIG. 6. Time dependence of the dynamical correction factor for the $S_{II} \rightarrow S_{II}$ benzene jump in Na-Y at 298 K.

FIG. 7. Ln|OCF| for benzene in Na-Y (Si:Al=3.0) at $T = 300$ K by KMC. Intracage motion gives rapid, incomplete decay while cage-to-cage migration gives slower, long time decay.

FIG. 8. Site-to-site jump activation energies perturbed by guest–guest interactions, approximated with parabolic jump model.

FIG. 9. Comparison between KMC and MFT for benzene in Na-X at three different temperatures, showing that three diffusion isotherm types emerge.

FIG. 10. Diffusion isotherm for benzene in Na-X at 468 K, by PFG NMR (scaled by 5), TZLC (scaled by 100) and by KMC simulations.

FIG. 11. GCMC adsorption calculation for benzene in Na-X, showing hysteresis at $T = 340$ K ($T^* = 0.73$).

FIG. 12. Simulated coexistence envelope for benzene in Na-X, giving $T_c = 370 \pm 20$ K ($T_c^* = 0.79 \pm 0.04$).

FIG. 13. Diffusion isotherms for benzene in Na-X by KMC-MSD and KMC-MFA (see text) at 468 K for various values of J, showing the signature of subcritical diffusion for $J = -0.07$ eV.

FIG. 14. Schematic of cluster formation in subcritical nanoporous systems, where the subcritical droplet spans many Na-X cages that are full of benzene.

FIG. 15. Schematic of a TCP simulation, with identical but differently labeled particles.

FIG. 16. KMC calculated self diffusivities in membranes of various thicknesses and anisotropies, η, using the TCP method. $\eta > 0$ shows normal diffusion for sufficiently thick membranes, while $\eta = 0$ (single-file) is strictly anomalous.

FIG. 17. Vacancy transport through an $L = 6$ single-file system, with A-particles (dark) and B-particles (light). Steps (i) through (vii) represent the passage of an "A-vacancy" from right to left, giving particle displacement of one lattice spacing in the opposite direction.

FIG. 18. Log-log plot of MSDs calculated with KMC and theory for an $L = 60$ single-file system; from simulation (solid line), MFT (left-most dotted line), single-file diffusion theory with slope of $\frac{1}{2}$ (dashed line), and compound diffusion theory giving slope of 1 (middle and right-most dotted lines).